THE PENNSYLVANIA STATE UNIVERSITY
SCHREYER HONORS COLLEGE

DEPARTMENT OF BIOMEDICAL ENGINEERING

MELANOMA EXTRAVASATION THROUGH THE ENDOTHELIUM AFFECTS FOCAL ADHESION DISASSEMBLY

VIKRAM ESWAR

SUMMER 2016

A thesis
submitted in partial fulfillment
of the requirements
for a baccalaureate degree
in Biomedical Engineering
with honors in Biomedical Engineering

Reviewed and approved* by the following:

Cheng Dong
Professor of Biomedical Engineering
Thesis Supervisor

William Hancock
Professor of Biomedical Engineering
Honors Adviser

Esther Gomez
Assistant Professor of Chemical Engineering
Faculty Reader

* Signatures are on file in the Schreyer Honors College.

ABSTRACT

Melanoma is the most serious type of skin cancer and becomes difficult to treat when it metastasizes to secondary locations in the body. The extravasation of malignant cells through the endothelial barrier is a highly intricate process, involving interactions between soluble cytokines and transmembrane ligand-receptors. Extensive work has been done to characterize the signaling cascade associated with endothelial gap formation during extravasation, specifically the breakdown of cell-cell junctions and cytoskeletal rearrangement mediated by activation of Src, a non-receptor tyrosine kinase. Src has been also implicated in focal adhesion turnover and assembly during cell spreading. This study aims to build on past experiments by developing a better understanding of endothelial gap formation during melanoma transmigration and the role that focal adhesions play in the process. To this end, traction force microscopy was used to measure forces exerted by two to six endothelial cells seeded onto 100 μm circles on 5 kPa polyacrylamide gels. Upon incubation of these micro-patterns with A2058 metastatic melanoma for 10 min, 45 min, and 90 min, measured endothelial forces were found to decrease with time. Using a similar experimental set-up, co-incubation with A2058 for 10 min, 45 min, and 90 min, endothelial micro-patterns were fluorescently stained for vinculin and F-actin. A statistically significant reduction in both focal adhesion (FA) number and total FA area per cell was observed at each time point compared to the negative control (no treatment) suggesting a close relationship between FA expression and traction stresses. Co-incubation experiments with a Src inhibitor, PP1, reversed this decrease in FA number and area after 90 min. Overall, these results propose a relationship between decreased traction forces and Src-mediated disassembly of focal adhesions during extravasation.

TABLE OF CONTENTS

LIST OF FIGURES

LIST OF TABLES

ACKNOWLEDGEMENTS

I would like to give thanks to my principal investigator and mentor, Dr. Cheng Dong, for his continued support and guidance throughout the research process and my undergraduate career. I would also like to express thanks to Dr. Gomez for her assistance in helping me with the experimental design and for the use of her laboratory. Thank you to Dr. Hancock for agreeing to be a part of my committee. I would also like to express my heartfelt gratitude to Virginia Aragon for her continued assistance from my very beginnings in the Cellular Biomechanics Lab and in helping me learn the necessary laboratory techniques. Finally, thank you to my friends and family for your compassion and support these past years.

ABBREVIATIONS

ADB	Antibody Dilution Buffer
BSA	Bovine serum albumin
CSB	Cytoskeleton stabilization buffer
FA	Focal adhesions
FBS	Fetal bovine serum
HPMEC	Human pulmonary endothelial cell
IL-8	Interleukin-8
MLCK	Myosin light chain kinase
PA	Polyacrylamide
PBS	Phosphate buffer saline
PDMS	Polydimethylsiloxane
TFM	Traction force microscopy
VCAM-1	Vascular cell adhesion molecule 1
VE-CADHERIN	Vascular endothelial cadherin
VLA-4	Very late antigen-4

Chapter 1

Introduction

1.1 Cancer

Cancer is the uncontrolled growth of cells. Fundamentally a developmental disorder, cell growth and replication is not regulated, allowing its mass proliferation through the organism. This is attributed to corruption of cellular DNA leading to abnormal gene expression and the inhibition of regulatory pathways that keep growth in check. Two types of genes in particular are responsible for cancerous growth: oncogenes and tumor suppressor genes. Oncogenes are derived from mutated forms of normal genes and their presence promotes uncontrolled cellular division and enhances survival.[1] As they are phenotypically dominant, a single copy is enough to promote cancer. Tumor suppressor genes are factors that inhibit proliferation and heavily regulate the cell cycle and apoptosis, a form of suicide.[1] Phenotypically recessive, inhibition of both alleles are necessary to cause uncontrollable growth. A combination of oncogenes and tumor suppressor genes, usually inherited from parent germ lines, is critical to the widespread proliferation of cells and explains certain people's predispositions to particular forms of the disease.[1]

Cancerous cells have many defining characteristics that differentiate them from their normal counterparts. First, cells develop an independence from growth factors, either stimulating their own receptors with synthesized growth factors as a form of autocrine signaling or stimulating neighboring cell receptors as a form of paracrine signaling.[2] Additionally, for these

cells, their rates of apoptosis are markedly reduced, particularly due to DNA damage from hyperproliferation.[2] Finally, certain cancerous lines have the ability to metastasize, a process that is poorly defined. This phenomenon allows the transport of cancerous cells to other areas of the body through the blood or lymphatic vasculature.[2] These characteristics are the most prevalent when describing the difficulties in developing viable treatment options.

1.2 Melanoma

Melanoma is a highly lethal form of cancer, found in the epidermis, or outer layer of skin. It is the most common type with an estimated incidence level of 3.5 million people.[3] The developmental risk for the disease has increased from 1 in 1500 in 1935 to 1 in 30 in 2009, leading to enormous costs for both practitioners and payors.[3] This disease is largely due to the rampant proliferation of melanocytes, cells found in the lower epidermal region of the skin, which create melanin, a dark pigment largely responsible for skin coloration. There are a wide variety of risk factors associated with melanoma, primarily family history, exposure to sunlight, presence of moles or blemishes, and fair complexion.[4] The exact causes have not been thoroughly elucidated; however, a relationship between UV light and lesion formation has been suggested.[5] One theory suggests that inflammation in the skin induced by sunburn acts as a promoter for viral and chemical carcinogens.[4]

The most common site of occurrence is on the surface of the skin, with fairer people having a higher genetic predisposition, although the disease can manifest in the bowels, back of the eye, or at the surface of mucosal membranes in the mouth or rectum.[6] While the lesions resulting from this condition are usually a darker tinge relative to normal skin color, certain types

can appear amelanotic, without the discoloration. Consequently, the most common case, superficial spreading, involves growth from a preexisting mole or blemish.[6]

Melanoma is not innately metastatic but develops this potential over time. During the first nontumorigenic phase, no lump or nodule forms. During this time, melanoma cells are contained entirely within the epidermis and are said to be in situ. The cells begin to grow into the lower dermal layers during the invasive radial growth phase. It is paramount that the growth be removed at this stage as further growth will make excision exponentially more difficult and possibly result in migration of cells to other parts of the body. In the next step, known as the vertical growth, or tumorigenic phase, melanoma begins to grow as a tumor within the dermis, creating an abnormal sphere of mutant melanocytes, as depicted in Figure 1.[7]

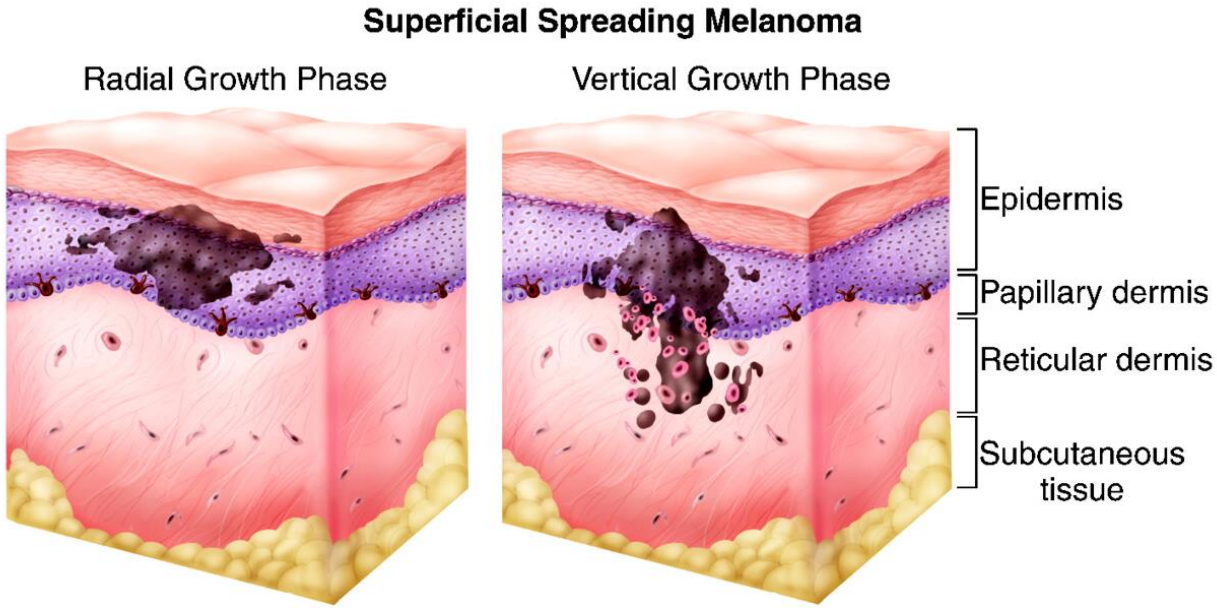

Figure 1. The first phase of melanotic growth is termed radial growth and results from cellular growth horizontally outward from a central nodule (*left)*. These cancerous cells are generally confined to the epidermis. Eventually, the vertical growth phase begins as the cells accrue metastatic potential (*right)* resulting in invasion of lower dermal layers and the basement membrane. Eventually, the growth reaches the vasculature, spreading to secondary sites in the body.[7]

It is at this time that lesions are characterized by asymmetry, border irregularity, color variation, and a diameter greater than six millimeters.[5] The most widely used treatment options are surgery/excisions, immunotherapy, the patient's own immune system in biologic therapy, and chemotherapy for very malignant cases; however, these methods do not necessarily guarantee complete remission if the lesion has spread to other parts of the body. For this reason, it is imperative that melanoma cells be stopped before migrating and subsequently complicate treatment.

1.2.1 Malignant Tumor Growth and Metastasis

Metastasis is a sequential series of steps that lead to the movement of cancerous cells from the original tumor site to new, healthy parts of the body. In this process, a group of cancerous cells detach from the main, primary tumor, circulate through the body's blood or lymphatic system and arrest at some secondary location where a new node begins to form.[8] In the first step, a mass of cells grows progressively, supplied by nutrients from simple diffusion. In order to grow to a size larger than 1-2 mm, angiogenesis, the creation of vasculature, must occur in order to allow convective transfer of essential molecules.[8] These capillaries are usually leaker than their normal counterparts and have been an avenue for drug therapy research for many years. As the mass size grows, tumor cells begin to grow through thin-walled vessels, typically in the lymphatic system or smaller capillaries, and eventually detach into the lumen allowing for passive circulation. This is done through degradation of the basement membrane with proteases.[8] Soon after, a small clump of tumorigenic cells embolizes and is carried through the circulatory system, although most cells are destroyed due to turbulent conditions. Eventually, the cells

become caught in the capillary bed of various organs or in the exposed subendothelial basement membrane. At this point, extravasation occurs and the cells proliferate within the new environment. The process repeats as angiogenesis begins and eventually, a host of new metastases forms.[8] It is important to note that through this entire process, metastatic cells must avoid immune host responses and adverse conditions. Despite these obstacles, sufficient cells expressing the appropriate oncogenes and membrane proteins can still produce a significantly large tumor (>5 mm).

1.3 Endothelial Barrier Disruption

Typically, endothelial cells form a semi-permeable barrier between blood and tissue, serving as an interface between the two mediums. Composed of adherens and tight junctions, this layer prevents movement of blood cells and other bodies into the extracellular space.[9] Normal function of this system allows the proper maintenance of circulatory and organ function. Nevertheless, substances can pass through the barrier through two routes: through the body of an endothelial cell (transcellular), or through opened contacts in the periphery (paracellular).[9] In a normal, homeostatic setting, both mechanisms maintain permeability; however, it has been found that increasing porosity is mainly achieved through modification of the paracellular route.[10] The increased permeability of the endothelial barrier has often been associated with wound healing, allowing facile movement of leukocytes and clotting factors to sites of inflammation.

Melanoma cells have been found to manipulate the permeability of this barrier through various means. This usually occurs during intravasation, from the original tumor site to the blood vessel, and extravasation, from the vasculature to a secondary site. The exact pathway by which

this cellular movement takes place is not clearly defined as many contributing factors complicate the process. However, recent efforts by Weidert et al. have found that a combination of disassembled endothelial cell-cell junctions and endothelial contractility play a significant role in migrating melanoma cells.[11]

1.4 Mechanism of Extravasation

Extravasation of melanoma cells into the tissues can roughly be broken down into four steps: adhesion to the vascular surface, force generation and retraction of endothelial cells, detachment and invasion into the surrounding tissue, and matrix composition remodeling via enzymes.[12] Migration is typically accomplished through a complex interplay of transmembrane proteins and secreted cytokine signals. Many studies have been conducted to better describe these signaling cascades.

1.4.1 Interaction of Transmembrane Proteins

VE-cadherin, an adherens junction protein, is a primary controller of vascular permeability, as determined through leukocyte transmigration experiments.[13] This membrane protein is bound to β- and α-catenin molecules which, in turn, are fixed to actomyosin bundles in the cytoplasm. As they are allosterically regulated proteins, phosphorylation of the cytoplasmic domain will decrease adhesion between extracellular dimers.[13] Additionally, rearrangements of the actin cytoskeleton, due to signaling proteins, form stress fibers that lead to the dissolution of the membrane junctions.[14]

Melanoma cells express a dimeric ligand ($\alpha_4\beta_1$) known as very late antigen 4, VLA-4, which binds to domains 1 and 4 on an immunoglobulin expressed on the apical side of endothelial cells: vascular adhesion molecule-1 (VCAM-1).[15] Recent work conducted by the Dong lab has shown the binding of these two molecules can directly lead to disassembly of VE-Cadherin.[15] Additionally, a high expression of the VLA-4 antigen can be seen to directly correlate with heightened levels of gap formation, proving its essential role in the mechanism.[14] VCAM-1 is upstream of several integral signaling proteins, primarily Rac1, Rho, mitogen activated protein kinase, and myosin light chain kinase, all of which aid in junction breakdown, as illustrated in Figure 2.

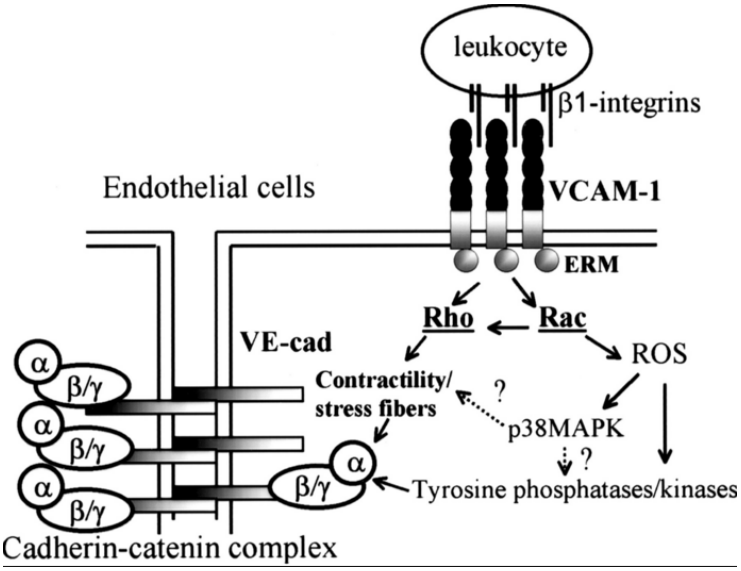

Figure 2. VCAM-1 signaling pathway upon stimulation by leukocytes. Rho and Rac signaling proteins are involved in the formation of stress fibers, which can lead to the dissolution of cadherin junctions through phosphorylation.[16]

1.4.2 Interaction of Soluble Signals

In addition to ligand-receptor interactions, melanoma secrete a wide array of pro-inflammatory cytokines to promote their proliferation and transport through the endothelial layer including IL-8, IL-1β, and IL-6. IL-8 is produced within a tumor microenvironment and has been proven to increase endothelial permeability in addition to allowing melanoma attachment to the vessel wall.[15] The secretion of this cytokine is found to be upregulated in melanoma cells compared to their noninvasive counterparts, which is a possible sign of their role in junction breakdown.[11] IL-1β was found to increase the secretion of cytokines such as IL-8 and intracellular adhesion molecule (ICAM-1) enhancing the melanoma cell's ability to adhere and migrate.[17]

1.4.3 Interplay of Ligand-Receptor Interactions and Soluble Signals

Experiments performed with inhibitors such as Cytochalasin D, an inhibitor of actin polymerization; PP1, an inhibitor of Src; and blebbistatin, an ATPase inhibitor, all resulted in reduced gap formation, suggesting an interplay of actin remodeling and junction disassembly.[11] Additionally, evidence has been shown to support the idea of crosstalk between remodeling and junction disassembly systems.[11] Due to similar characteristics between melanoma and various other cancer lines such as breast, ovarian, pancreatic, or prostate, particularly in their expression of VLA-4 and secretion of inflammatory cytokines, there is strong evidence to extrapolate the extravasation mechanism described to these other types.[11]

1.5 Force Production in Endothelial Cells

It has been found that endothelial cells generate anisotropic stresses on a particular substrate, specifically, forces with a front-back polarity, likely due to matrix remodeling and tissue morphogenesis.[18] Stress fibers are largely responsible for this and consist of 10-30 actin filaments bundled together, held by the protein α-actinin.[19] During contraction, myosin heads hydrolyze ATP and "walk" along actin filaments, causing antiparallel filaments to slide past each other, inducing contractile forces. This relationship is largely governed by the phosphorylation of myosin light chains (MLC) through myosin light chain kinase (MLCK) at serine and threonine residues, resulting in a change of tertiary structure and favoring contractile movement.[20] In the opposite direction, myosin light chain phosphatase (MLCP) dephosphorylates myosin, subsequently decreasing tension and contractile forces.[20] Therefore, a balance between these enzymes is necessary for control of the total force exerted by a cell. It has also been found that the binding rates of actin and myosin are force-dependent with larger tensile forces boosting actin recruitment and increasing stress fiber diameter.[21]

1.6 Focal Adhesion Expression

One method in the study of cellular contractility and adhesion to an extracellular matrix (ECM) is through the presence of focal adhesions. Despite the widespread research done on their form and function, the relationship between their expression and endothelial permeability is not clearly delineated. Focal adhesions contain integrins, transmembrane proteins that tether the cellular cytoskeleton to a substrate. Heterodimeric integrins possess a large extracellular and short intracellular domain, playing a role in reforming the actin cytoskeleton and acting as a

mechanism for mechanotransduction. The proteins not only interact with compounds on the ECM and bundles of actin filaments on the cytoplasmic side, but transmit forces and chemical signals between the cell and the matrix.[22] This is a result of two different types of signaling: inside-out and outside-in. In the former, signals received by other receptors trigger an intracellular signaling cascade that recruits focal adhesion components to integrin complexes.[23] In the latter, ligand binding to a specific integrin can lead to clustering through changes in integrin-ligand affinity.[23] This bidirectional transduction pathway allows cells to manipulate the surrounding substrate while simultaneously changing protein expression to better adapt to its surroundings.

Additionally, there are many cytoplasmic proteins that are responsible for a focal adhesion's function. Talin binds to activated integrin β-subunits to the actin cytoskeleton and promotes cytoskeletal crosslinking through vinculin recruitment.[23] Focal adhesion growth is achieved through binding of vinculin and can also reinforce crosslinking of the cytoskeleton.[23] α-actinin is thought to have a similar role as talin, localizing to focal adhesions and providing additional stability; however, its exact function is not clear as it is difficult to detect through immunofluorescence staining.[22] Figure 3 illustrates the protein structure of a focal adhesion and the relative binding locations of component proteins.[23]

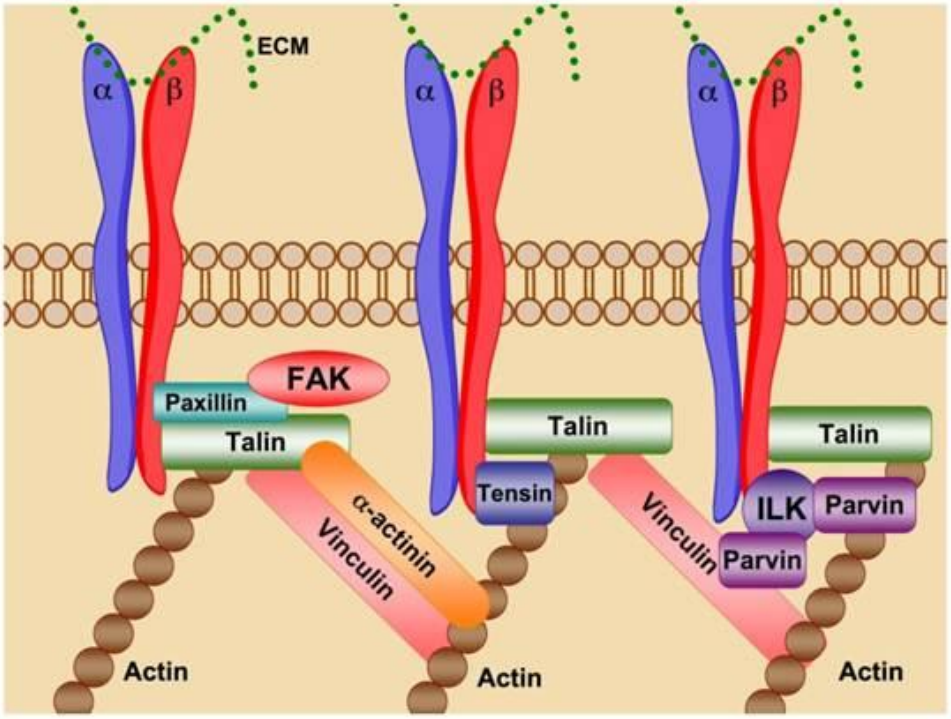

Figure 3. Protein composition of focal adhesions. Talin binds to both integrin and the actin cytoskeleton with vinculin and α-actinin providing a crosslink. ILK and parvin creates a core scaffold for adhesion formation and maturation. FAK and paxillin are responsible for initial formation of the FA and provide additional stabilization.[23]

1.6.1 Focal Adhesion Assembly/Disassembly

Focal adhesions are dynamic constructs, capable of being created and degraded as a cell moves through its environment. With different components recruited at different times, elucidating the exact dynamics has been a challenge. As a cell moves, it has been found that paxillin and α-actinin are the first to localize in membrane protrusions, likely serving a signaling and recruitment role.[25] During this formation stage, there is low expression of vinculin and focal adhesion kinase (FAK). Eventually, vinculin and FAK are recruited, contributing to the overall mechanical stability of the focal adhesion and regulating contractile stress generation. At these later contractile stages, there is a significant increase in vinculin, FAK, and α-actinin

expression.[25] It has been found that the initial formation of focal contacts is a result of small Rac1 GTPases with maturation of focal adhesions resulting after activation of Rho proteins.[24] As seen in Figure 2, Rho is also implicated in stress fiber formation and adhesion expansion, suggesting an important interplay between actin dynamics and focal adhesion formation.[16] When bound to GTP, Rho is active and phosphorylates downstream molecules, such as $PIP_{2,}$ which has been proven to promote actin polymerization by dissociating inhibitory molecules and results in the formation of stress-fiber bound focal adhesions.[22] Figure 4 illustrates the general mechanism by which a cell first makes contact with a substrate and forms adhesions. When a cell is motile, the adhesions form and disassemble within a span of about 80 seconds.[22] After a period of time, a small percentage of nascent focal adhesions can mature, becoming passive anchorage devices that maintain the spread morphology. The heightened levels of tyrosine phosphorylation in these structures results in increased levels of zyxin and stress fiber polymerization.[22]

Focal adhesion kinase (FAK) is a pivotal protein in both the construction and disassembly of focal adhesions. This molecule is activated by growth factors and integrins during migration and can act as a regulator of motility. At focal adhesions, FAK acts as an adaptor, recruiting other proteins to the adhesion site or directing its deconstruction. Its activation occurs through autophosphorylation of the Tyr-397 residue, resulting in its recognition by SH2 domains of the Src family kinases. These proteins also serve a regulatory role, influencing the activity of Rho-family GTPases.

In order to be motile, a cell must be capable of turning over and disassembling its focal adhesions. Typically, integrin clusters at the rear of the cell are endocytosed and sent to the leading edge. Studies have found that both Src and FAK are crucial elements of adhesion turnover.[24] An important component of focal adhesion assembly and disassembly is the tyrosine

phosphorylation of FAK; however, there is no consensus on its effect on vascular permeability as it has proven to both enhance barrier function and cause dysfunction.[26] Mice endothelial cells subjected to a FAK knock-down were found to increase the number and size of observed focal adhesions, the formation of a tighter and more cohesive monolayer, and exhibit more significant localization of VE-Cadherin to the membrane without any changes in concentration of the molecule.[26] These studies are a prime example of the complex associations between endothelial junctions, stress fiber formation, and focal adhesion expression.

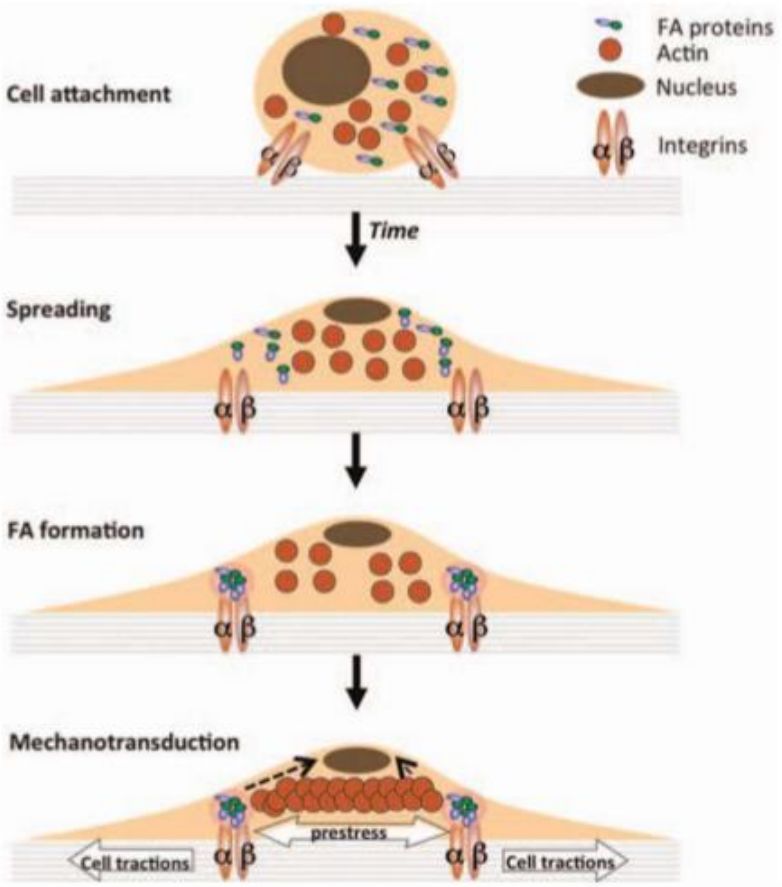

Figure 4. Cell attachment to substrate and sequential adhering through the construction of focal adhesions. After the adhesions have formed, mechanotransduction occurs allowing cells to exert forces on a substrate while receiving input from the surroundings.[27]

1.7 Src Family Kinases

Src is a cytoplasmic tyrosine kinase that is involved in many different cellular mechanisms that promote survival, angiogenesis, migration, and proliferation. These proteins are 52-62 kDa in size and are composed of six functional regions, all of which determine the different mechanisms by which the protein acts: the Src homology (SH) 4 domain, the unique region, the SH3 region, the SH2 domain, the catalytic domain, and a short, regulatory tail.[28] There are three ubiquitous groups of the Src protein tyrosine kinase family: Src, Fyn, and Yes. The absence of these proteins results in cells with impaired migration and an altered distribution of focal adhesions.[29]

This study focuses on Src's role in cellular adhesion and spreading. It has been suggested that Src kinases are involved with focal adhesion dynamics, particularly with their disassembly. These proteins can be activated by various receptors, including integrins, and are able to phosphorylate tyrosine residues Tyr-587 and Tyr-581 in the activation loop of FAK, resulting in FAK's complete, maximal activation.[30] A recent study found that Src-dependent FAK phosphorylation is required for focal adhesion turnover and cell migration.[29] One notable result of the newly formed Src-FAK complex is the activation of Grb-2 and the ERK2 pathway leading to phosphorylation of FAK by ERK2 and subsequent FAK dissociation from paxillin.[31, 32] The complex also allows for the recruitment of two important proteins: paxillin and p130Cas.[31] The binding of p130Cas allows for the formation of lamellipodia, or cellular protrusions, and integrin clustering through the Rac pathway while ERK-2 phosphorylated paxillin can bind with other FAK molecules and move to newly formed focal adhesions.[31] This signaling cascade is depicted visually in Figure 5.

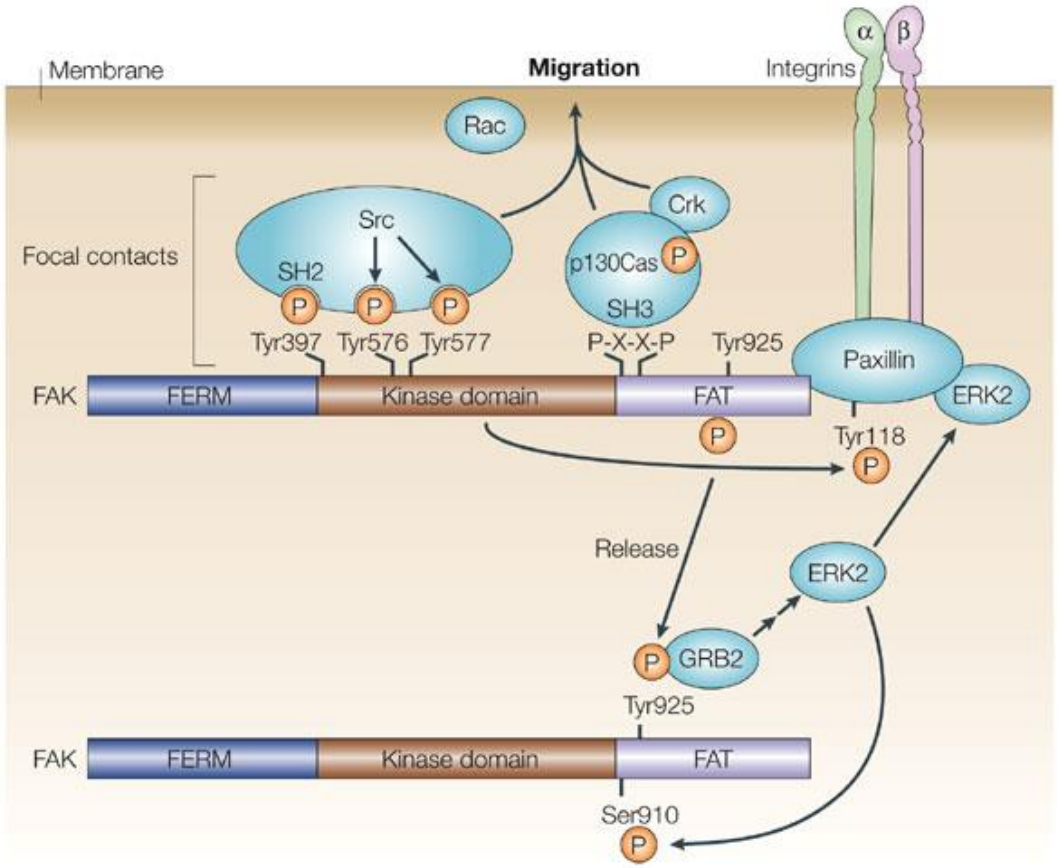

Figure 5. Signaling cascade resulting from Src-FAK complex formation and specific phosphorylated residues. Activation of p130Cas leads to Rac pathway and formation of lamellipodia while paxillin binds to FAK and begins adhesion formation at new sites through the ERK2 cascade.[31]

Recent studies have delved further into the oncogenic potential of the Src protein. v-Src causes uncontrollable cellular growth in chicken embryo fibroblasts and lead to the discovery of retroviral oncogenes. Many of its targets are located on the cell periphery, particularly localized around the cytoskeletal network and focal adhesions.[33] It was noted that v-Src specifically phosphorylated $pp125^{FAK}$, a kinase present at adhesion sites, causing an initial surge in its activity but subsequent degradation and cell detachment and rounding.[32] This study illustrates the effects of pathogenic Src and its role in adhesion disassembly.

1.8 Principles of Traction Force Microscopy

Traction force microscopy (TFM) is a useful technique for measuring the forces exerted on a substrate by a cell. This, in turn, provides key insight into the intracellular mechanisms regarding contractility in real-time upon application of a stimulus. TFM is advantageous for many biological and physical applications because it has no inherent size or force scale allowing a wide range of experiments to be performed and interfacial forces to be easily spatially-resolved.[18] In this technique, microscopic, fluorescent beads are suspended in a hydrogel of physiological stiffness. After seeding the cells, natural traction forces are generated causing a deformation of the gel and subsequent bead displacement. Analytic software can convert this displacement to a generated force based on the stiffness and scale of the object. Standard bright field or fluorescent microscopy is used for measuring bead displacements in-plane; however, obtaining 3D images requires the use of confocal microscopy.[18] Care must be taken to ensure there is sufficient contrast between the beads and background for optimal resolution.

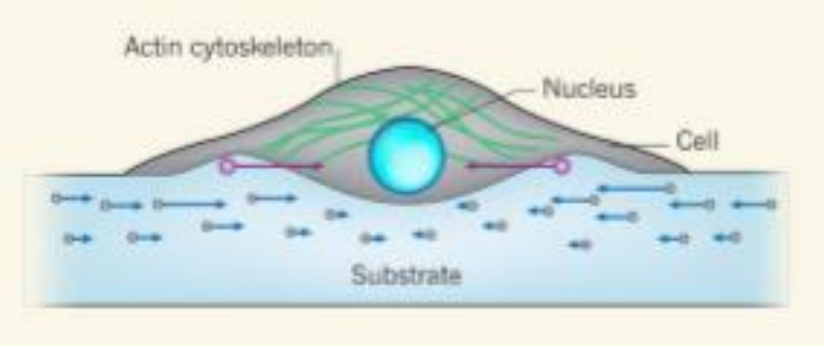

Figure 6. Bead displacement (blue arrows) can be used to calculate the force exerted over a certain area (red arrows).[35]

1.9 Experimental Aims and Significance

Much of the work conducted so far in Dr. Dong's lab has been studying the signaling cascades involved in melanoma metastasis. As has been described, previous studies have already proven the interplay between junction disassembly, actin remodeling, and contractility, confirming the role that ligand-receptor interactions and soluble signaling factors have in this process.[11] Interestingly, the study of endothelial contractility on various substrates of physiological relevance has only been conducted based on stimuli from leukocytes, which undergo different extravasation mechanisms from cancerous cells.[36] Consequently, due to the wide variety of factors and proteins involved, there is still much work to be done in mapping the exact mechanism by which melanoma cells extravasate so readily compared to host immune cells.

Previous studies, in the form of an unpublished manuscript, conducted in our lab have already found that co-incubation of melanoma and endothelial cells leads to elevated activity of Src and subsequent gap formation within the endothelial barrier. The present study builds upon these past experiments to develop a better understanding of endothelial contractility that includes activation of the Src kinase.

The first experimental aim, completed through traction force microscopy experiments in conjunction with Virginia Aragon, is to better characterize endothelial contractility and provide a temporal representation of extravasation. The second aim, achieved through immunofluorescence staining of vinculin in human pulmonary endothelial cells incubated with metastatic melanoma, is to quantitatively describe the presence of focal adhesions as a function of time and also lend insight into FA expression as cellular Src activity changes. As the presence

of FAs usually occurs in concert with the formation of stress fibers, these experiments in conjunction with TFM, will shed light on the role that focal adhesions play during metastasis.

Overall, this study will allow further understanding of the mechanism by which melanoma invades secondary locations in the body, specifically the roles that Src and focal adhesions play, and suggest a new, possible source of therapy through control of these proteins.

Chapter 2

Materials and Methods

2.1 Cell Culturing

Cell lines were kept in treated polystyrene petri dishes at 37 °C and 5% CO_2. Human pulmonary microvascular endothelial cells (HPMECs) were a generous gift from Dr. Kirkpatrick from the Institute of Pathology at the Johannes Gutenberg University. These cells were cultured in Media 199 supplemented with 10% Fetal Bovine Serum (FBS), 2mM L-Glutamine, 100U/mL Penicillin, and 100µg/mL Streptomycin. Every two days and before any experiments were conducted, cells were placed under a bright field microscope to determine confluence. If cells were determined to exceed 75% confluency, the media was aspirated out and cells were washed once with 5 mL of 1x phosphate buffer saline (PBS). The cells were then detached using 0.05% Trypsin-EDTA and centrifuged for 5 min at 1500 rpm at 10 °C. Cells were then passaged into another treated polystyrene dish at a 1:3 ratio.

Malignant A2058 melanoma cells, courtesy of American Type Culture Collections, were cultured in Dulbecco's Modified Eagle Medium (DMEM) supplemented with 10% FBS, 2mM L-Glutamine, 100 U/mL Penicillin, and 100 µg/mL Streptomycin. Confluency was monitored daily with passaging completed when coverage exceeded 80% of the bottom. The same protocol for passaging HPMEC cells was used here; however, cells were split in a 1:10 ratio due to the faster growth rate. For both types of cells, culture dishes between 45% and 90% confluency were

used for experimentation. All media, supplements, and antibodies were purchased from Invitrogen unless otherwise specified.

2.2 Polyacrylamide Gel Synthesis

Polyacrylamide (PA) gels for traction force experiments were all stored in petri dishes filled with 1x PBS at 4 °C. First, 22x22 mm square glass slides were submerged in 0.1 N NaOH for 15 minutes. To do this, slides were placed one by one in a 10-cm polystyrene dish to ensure even coverage on both sides and prevent them from sticking together. Each side of a slide was then rinsed three times with distilled water and any excess liquid was subsequently aspirated out. Slides were checked for any white, flaky discolorations as a result of treatment, and dirty ones were discarded. In a fume hood, slides were placed in a 2% aminopropyltrimethoxysilane (APTMS) in acetone solution for 30 minutes. Each side of a slide was rinsed three times with acetone and left to air dry completely. Care was taken to ensure unwashed slides were completely submerged in acetone throughout the process. Next, slides were left in a 0.5% glutaraldehyde in water solution for 30 minutes. Slides were then rinsed with distilled water and left to dry with any excess liquid aspirated out. Care was taken to ensure no dark, red discolorations were visible in the center of any slides due to improper washing.

A 5 kPa gel was chosen because of its accurate representation of the stiffness of the sub-endothelial layer.[36] To make this, a 1 mL solution consisting of 5.5% acrylamide (137.5 µL of a 40% acrylamide solution, BioRad), 0.15% bis-acrylamide (75 µL of a 2% bis solution, BioRad), and distilled water (787.5 µL) was first left in a desiccator for 30 min. During this time, a 10% by weight ammonium persulfate (APS, BioRad) solution in water was made. Additionally, 5 mm

circular cover slips were treated with Rain-X® three times on each side and left to dry for 30 minutes. The treatment allowed facile cover slip removal later on due to increased hydrophobicity. After desiccation, 0.5 µL of tetramethylethylenediamine (TEMED, BioRad) and 5 µL of the previously made APS solution were added to the acrylamide solution, which was then mixed vigorously using a 1000 µL pipette. 8 µL of this was then pipetted onto the center of each slide and the previously treated Rain-X® cover slips were placed on top. The gels were allowed to polymerized for 45 minutes, or until the solution solidified, before being stored in 1x PBS and placed in a 4 °C refrigerator overnight.

The next day, another polyacrylamide solution of the same concentration was synthesized and desiccated while 15 mm cover slips were treated with Rain-X® and left to dry for 30 min. As before, 0.5 µL of TEMED and 5 µL of a 10% by weight APS solution were both added along with 5 µL of a 0.2 µm FluoSpheres® carboxylate-modified microsphere solution (Life Technologies) to the acrylamide solution. These microspheres have an excitation wavelength of 580 nm and an emission wavelength of 605 nm, appearing red under fluorescent microscopy. After, 12 µL of the solution was pipetted directly onto the previously made gel and covered with the 15 mm cover slip. After being allowed to polymerize for 45 min, or until the solution solidified, gels were checked under a fluorescent microscope to ensure uniform bead distribution throughout. These were then stored in a 1x PBS solution at 4 °C for later use.

Figure 7 shows examples of fluorescent images highlighting bead density. Figure 7A represents the ideal bead placement, with uniform coverage and no distinguishing clumps. Figure 7B exhibits a pattern often found closer to the edge of a slide where beads aggregate, displaying bright streaks. These areas cannot be analyzed as there is not sufficient resolution to determine displacement. Figure 7C shows gaps as a result of non-uniform polymer application. These holes

also inhibit accurate readings due to large areas with no discernible displacement. Polyacrylamide gel synthesis had to be tailored appropriately through modification of the application time and placement of the coverslip to avoid these latter two distributions.

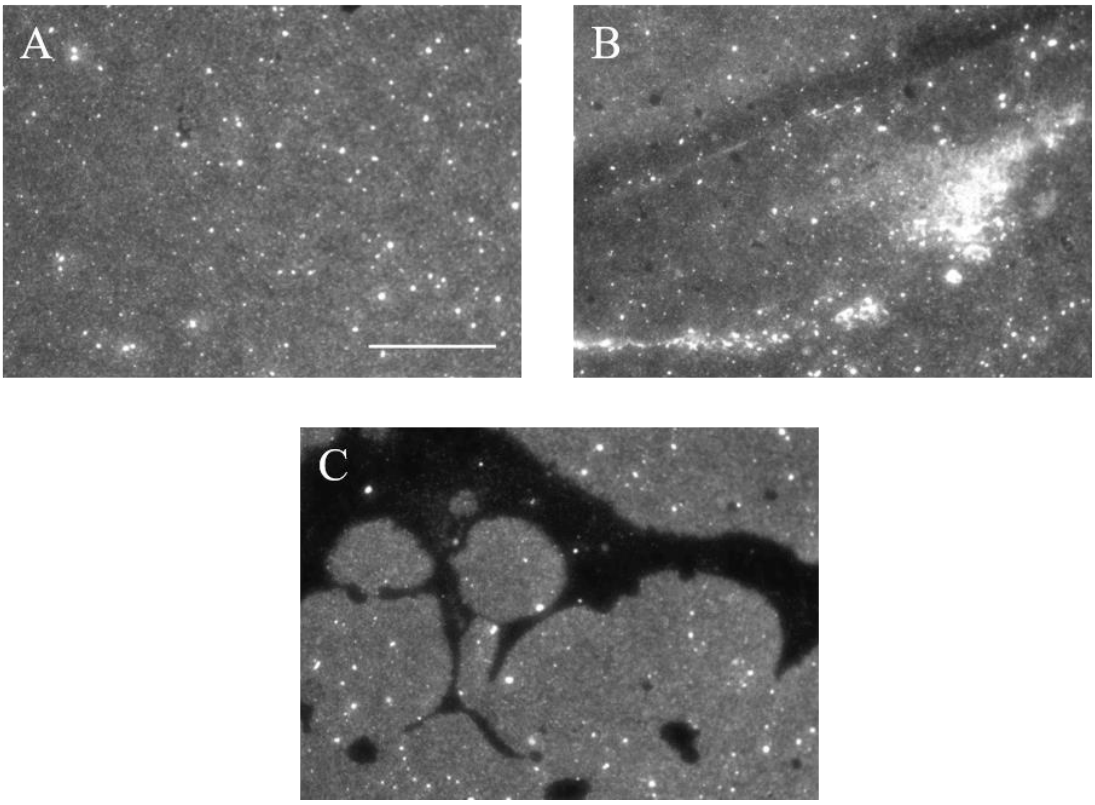

Figure 7. Fluorescent bead images of 5 kPa PA gels at 20x magnification. (A) Optimal distribution, (B) Streaks due to bead aggregation, (C) Large gaps due to non-uniform polyacrylamide solidification. Scale bar: 50 µm

For the synthesis of polyacrylamide gels used during immunofluorescence staining, the same procedure above was used; however, only one layer was applied. After making the acrylamide solution, 20 µL was pipetted onto a 22x22mm glass slide with a 15mm circular Rain-X® cover slip placed on top. After polymerization, the gels were stored in PBS at 4 ºC.

2.2.1 Micro-patterning

Polydimethylsiloxane (PDMS) gels were first made by mixing a base and a curing agent in a 10:1 ration (80g and 8 g, respectively) thoroughly for 2 minutes. The mixture was placed in a desiccator and degassed until all existing bubbles in solution were gone. Throughout this process, care was taken to relieve pressure before the container overflowed. Half of the solution (~40 g) was then carefully poured over a silicone micro-patterned wafer with an array of 100 µm diameter circular shapes. The other half was poured over a silicone piece that had no patterns. Both molds were then placed in a 63 °C incubator overnight and later cut into small squares, roughly 2x2cm, or relatively the same size as the polyacrylamide gels made previously. Similarly sized squares were cut from the smooth PDMS.

Next, a 10 µg/mL fibronectin in pH 8.5 modified HEPES solution was added dropwise to the top surface of the pattern-less PDMS gel pieces and spread out to evenly cover the surface with a pipette tip. This solution was then left to incubate at room temperature for 2 hrs. During this time, polyacrylamide gels made previously were treated with 200 µL of a 0.5 mM Sulfo-SANPAH (Thermo-Fisher) solution made in pH 8.5 modified HEPES. Then, all PA gels were left to incubate in a UV crosslinking chamber for 10 minutes. After, each PA gel was rinsed with 200 µL of HEPES (pH 8.5). This procedure was repeated again, with 200 µL of Sulfo-SANPAH added to each PA gel, cross-linking treatment, and another rinse. After, the gels were left on a hot plate at 60 ºC for 15 min or until they were completely dry. Then, the micro-patterned PDMS pieces were placed in a Jelight UV-ozone (UVO) cleaning oven for 7 min. This part of the procedure increased the PDMS substrate's wettability and hydrophilicity, allowing for facile micro-patterning later on.

Next, the fibronectin-coated PDMS gels were rinsed with sterile PBS. A handheld blower was then used to gently air dry the gel surfaces. In the sterile hood, the UVO-treated, patterned PDMS gels were placed face down on the fibronectin-coated PDMS gels and gentle pressure was applied to the corners with a set of tweezers. The top gel was then removed with extreme care taken to not smear the newly minted pattern. The bottom, smooth gel was then inverted and placed face down flush on the dried PA gel and left for 2 min. After careful removal of the PDMS gel with tweezers, fibronectin circles with a diameter of 100 μm on the 5 kPa PA gels were left. The general schematic for micro-patterning is shown in Figure 8 from the initial formation of the PDMS polymer to the application of the final circular fibronectin patterns. For seeding, counting with trypan blue was used to obtain a solution of 4,000 HPMEC cells per cm^2. The cell solution was then added dropwise, with an ideal volume between 50-100 μL. The gel was checked the next day for proper adhesion.

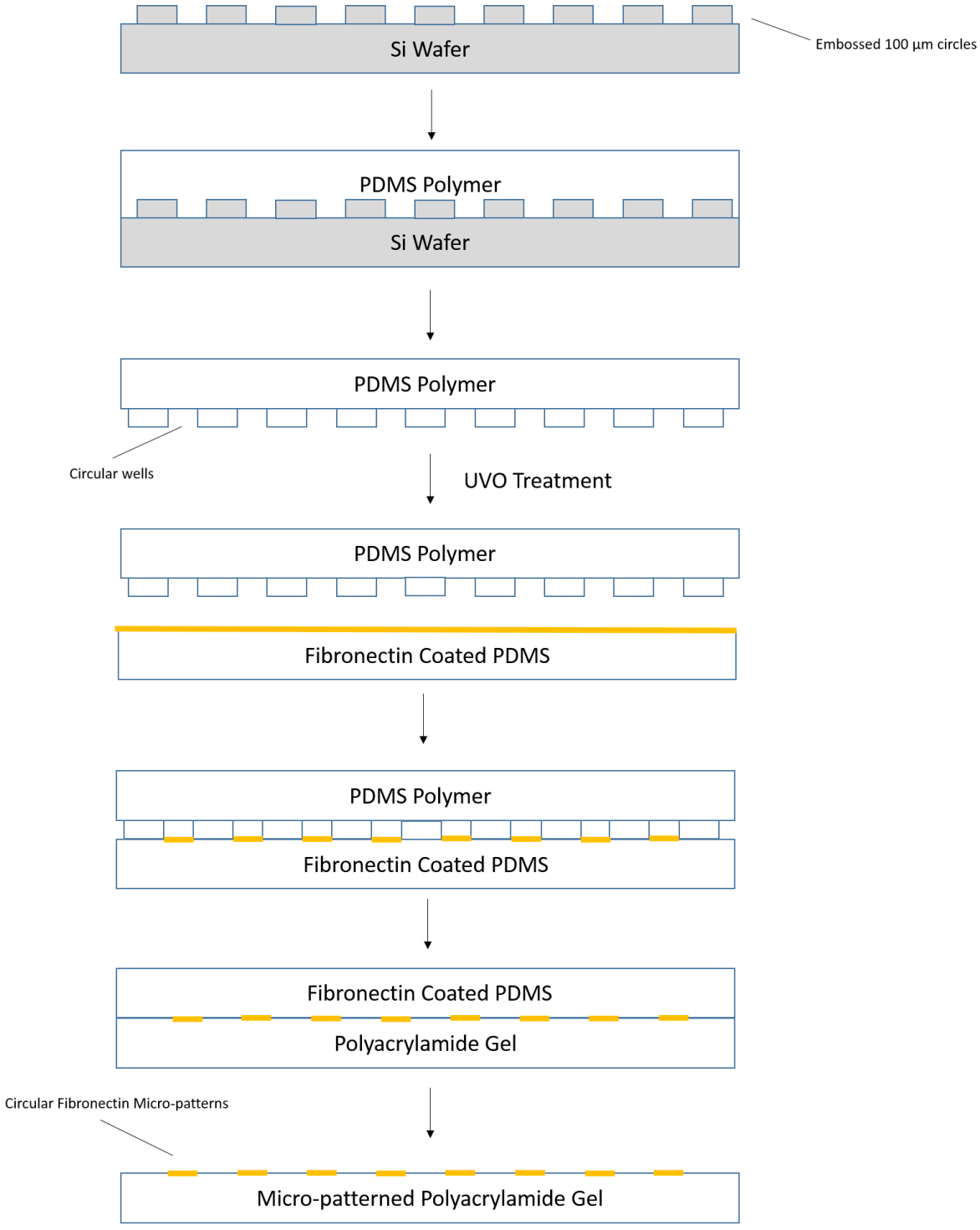

Figure 8. The overall procedure for micro-patterning. Gold lines indicate fibronectin. First, a PDMS pre-polymer is poured over a silica wafer, leaving 100 µm circular wells in the gel. After, the patterned PDMS gel undergoes UVO treatment and is then placed on smooth PDMS coated with a fibronectin solution. After removal of the patterned layer, the smooth gel is placed face down on sulfo-SANPAH treated polyacrylamide, leaving the final product.

2.3 Traction Force Microscopy

The day before any experiments were conducted, the existing media was aspirated from HPMEC micro-patterned PA gels and replaced with 2% FBS supplemented Media 199. The day of the experiment, 12 µL of this same media was pipetted onto a 5 cm petri dish. Then, vacuum grease was applied to the bottoms of the four corners of the micro-patterned PA gel slide, which was gently placed on top of the previously added media. 2 mL of reduced serum 2% FBS Media 199 was then pipetted onto the polyacrylamide with extra care taken to ensure complete coverage.

The experiments took place inside a live cell control chamber that maintained a 37 °C, 5% CO_2, and 75% humidity environment. Images were recorded using a Nikon Eclipse Ti-E inverted microscope equipped with Photometrics Cool SNAP HQ CCD camera and a 20x objective. For each negative control gel where endothelial cells were left alone, six to seven locations were defined using bright field microscopy with their coordinates recorded. Ideal images had one to three micro-patterned circles of HPMEC cells with no outside detritus or cell growth. At each location, images were first focused manually in bright field, autofocused in Tx Red (580nm), and only then were both channels captured. This was repeated every 10 min over a 90 min period. After, 1 mL of a 1 % by weight SDS solution was added dropwise to lyse all cells. Bright field and fluorescence images of the cells and beads were taken again after cell detachment from the substrate creating a null image. Each fluorescent time point image was then compared to this last “null” image to measure bead displacement.

For co-incubation experiments, A2058 melanoma cells were first counted and diluted to a desired density of 40,000 cells/mL. For each experimental trial, melanoma cells were added to three HPMEC micro-patterned PA gels and left in an incubator at 37 °C and 5% CO_2 for either

10 min, 45 min, and 90 min. A fourth negative control gel (no treatment) was used for comparison. The same procedure for image capture mentioned previously was used again, with bright field and fluorescence images taken before and after cell detachment. To acquire time course images for the A2058 control experiment seen in Figure 10, cells were imaged in bright field at the desired time points directly after addition of A2058. While the automated NDX software was able to switch from location to location automatically, extreme caution was used to manually realign the corners of fluorescent null images to match the corners of pictures taken before addition of SDS. Improper alignment resulted in erroneous traction forces and improbable stress distributions. The final forces were calculated using the LIBTRC software package developed by Dr. Micah Dembo from Boston University. Final forces are reported as normalized values based on negative controls (endothelial cells alone).

2.4 Immunofluorescence Staining of Vinculin

First, micro-patterned HPMEC cells were seeded at a concentration of 40,000 cells per cm^2 onto fibronectin micro-patterned PA gels. The day before experimentation, the existing media was aspirated out and replaced with 2% FBS reduced serum Media 199. The next day, endothelial cells were incubated with A2058 melanoma on three separate gels, one for 10 min, one for 45 min, and one for 90 min. Immediately after the experiment, 1mL of a cytoskeletal stabilization buffer (CSB) was added to each gel at room temperature for exactly 1 min. This pH 6.8 buffer was composed of 50 mM NaCl, 0.5% Triton X-100, 10 mM PIPES, 2.5 mM $MgCl_2$, 1 mM EGTA, and 0.3 M Sucrose. Directly after, the gels were fixed with a 4% paraformaldehyde fixation buffer for 15 min at room temperature. Each gel was then washed once with 2 mL of 1x

PBS and then a permeabilization/blocking buffer, consisting of PBS, 3% bovine serum albumin (BSA), 10% goat serum, and 0.1% Triton X-100 was added. The gels were then left to incubate for 1 hr at room temperature. After, a wash was performed once with PBS for 5 min.

Next, each PA gel was incubated with 100 µL of an antibody solution consisting of a primary Ab for vinculin (1:200, Thermo-Fisher) and an antibody dilution buffer (ADB), containing PBS, 3% BSA, and 0.1% Triton X-100, for 1 hr at 4 ºC. Each gel was then washed once with PBS for 5 min and subsequently incubated with 150 µL of a secondary antibody solution (fluorescently tagged Goat anti-Mouse in ADB, 1:1000 dilution) for 1 hr in the dark at room temperature. After another wash with PBS for 5 min, 150 µL of an F-actin staining solution was added (Phalloidin-Atto 565 in ADB, Thermo-Fisher, 1:100 dilution) for 30 min protected from light at room temperature. Gels were then washed once with PBS for 5 min and then counterstained with 150 µL of a solution containing Hoescht stain in PBS (1:5000 dilution). After one final wash with PBS for 5 min, cells were mounted on microscope slides using 100 µL of Fluoromount-G (Southern Biotech) and left covered overnight at 4 ºC. Images were recorded using a Nikon Eclipse Ti-E inverted microscope equipped with Photometrics Cool SNAP HQ CCD camera and a 40x objective. Intact micro-patterns were selected that contained between 2-6 HPMEC cells. For co-incubation experiments, micro-patterns were selected based on whether endothelial cells were in direct contact with melanoma. Images were then taken in GFP, TxRed, and DAPI channels. The data reported is the result of four independent replicates.

2.4.1 Focal Adhesion Analysis

Micro-patterns were readied for analysis using ImageJ with subsequent processing done through the Focal Adhesion Analysis Server (FAAS) by Dr. Shawn Gomez at the University of North Carolina-Chapel Hill. Preliminary analytic methods attempted to isolate each cell in a micro-pattern, defining a boundary through the Freehand Selection tool in ImageJ. However, as shown in Figure 9, these borders lead to a large conflation in focal adhesion number and total area, likely due to the erroneous recording of FAs skewing final results. During these trials, it was also found that noise around the nucleus was also misidentifying adhesions; however, later trials that used the cytoskeletal stabilization buffer were able to cut this down significantly.

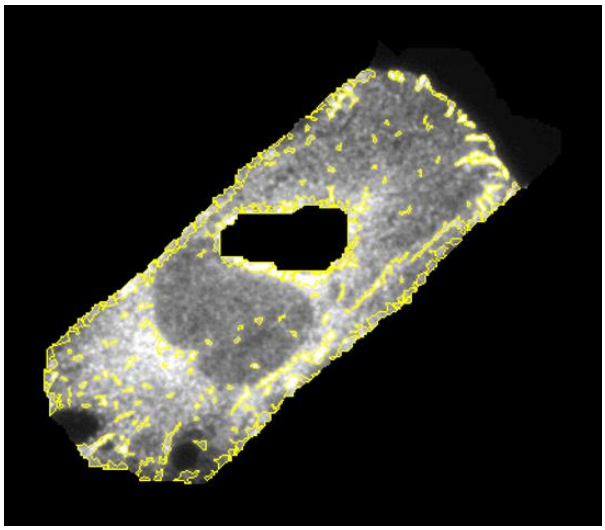

Figure 9. Attempt at single-cell analysis of focal adhesion expression. Each adhesion site is encircled in yellow. The borders, as drawn in ImageJ, lead to misreading of adhesion expression. This can be especially observed within the circular excision in the middle of the cell.

In ImageJ, all the micro-pattern images from a specific gel were made into one stack. Then, the localized contrast of each image was enhanced through equalization of the histogram. This pre-processing step allowed better resolution and accurate detection of adhesions through the FAAS. Through the server, the detection threshold was set at 2.5, slightly above the default

of 2. This setting applies a high pass filter to images, considering pixels above a certain intensity to be part of an adhesion while lower ones are considered background. The minimum individual adhesion size was set to 20 pixels, as values below tended to be noise, while the maximum size was set to 400 pixels. This upper bound correlates to an area of 10 μm^2, an area twice as big as larger, mature focal adhesions. Due to the inability to characterize adhesion expression for a single cell, the entire micro-pattern was analyzed with the server. The output from the server was a list of individual FA areas across the total pattern, and the following two equations were used to calculate the number of adhesions per cell (Eqn. 1) and the total adhesion area per cell (Eqn. 2):

$$\frac{Total\ number\ of\ focal\ adhesions}{Number\ of\ cells\ in\ micropattern} = \#\ of\ adhesions\ per\ cell \quad \text{Eqn 1.}$$

$$\frac{\sum Individual\ focal\ adhesion\ areas}{Number\ of\ cells\ in\ micropattern} = Total\ adhesion\ area\ per\ cell \quad \text{Eqn 2.}$$

2.5 Inhibition Studies

Experiments that required the inhibition of Src were performed after adding inhibitor PP1 in 2% FBS Media 199 (30 μM, Sigma) for 2 hrs before. After this, media was aspirated and fresh 2% FBS Media 199 was added before co-incubation. Immunofluorescence experiments were conducted over two independent replicates, each consisting of two negative control gels, with endothelial cells alone, and two 90 min co-incubation gels with A2058.

2.6 Statistical Analysis

One-way ANOVA tables with subsequent Tukey post hoc tests were used to determine statistically significant differences in means between experimental time points. All data are expressed as the mean ± SEM.

Chapter 3

Results

3.1 HPMEC-A2058 Contractility Experiments with TFM

Traction force experiments were conducted to study changes in endothelial contractility upon direct interaction with A2058 metastatic melanoma. A series of preliminary experiments, one isolating forces produced by HPMECs and one studying contractility of melanoma, were first conducted to obtain a base line level of contractility for later comparison. In the first, A2058 cells were added to fibronectin-coated PA gels in order to assess if cells adhered to the surface and caused measurable force production on their own. Cellular attachment was confirmed after lightly shaking the petri dish and noting no cellular displacement. Figure 10 shows four representative bright field images from a time course experiment at time 0 min, 10 min, 45 min, and 90 min. In all, six different areas were selected randomly across a PA gel. No traction forces were recorded at any point during the experiment. This was likely due to the inability of a single cell to induce a significant deformation of the gel.

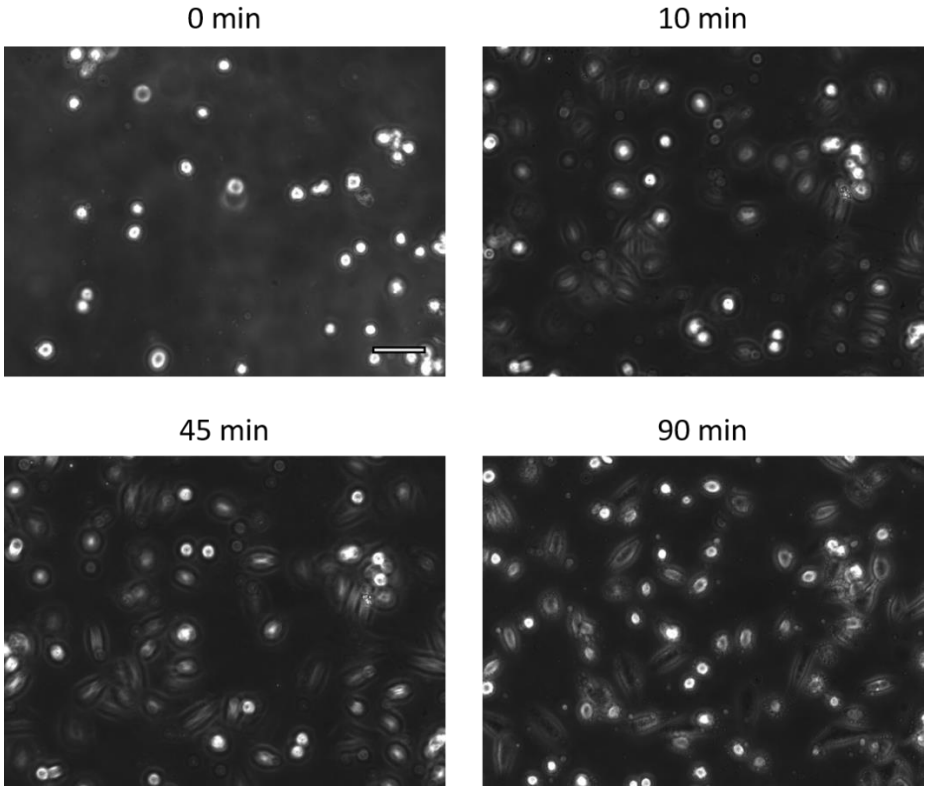

Figure 10. Representative time course images of A2058 cells on PA gels at 0 min, 10 min, 45 min, and 90 min. Scale bar: 50 μm.

Negative control experiments were conducted with HPMEC cells alone to quantify a baseline contraction level and ensure no significant deviations were present during the 90 min experimental time period. As mentioned previously, single cell contractile forces were not significant enough to be recorded, so micro-patterns, as seen in Figure 11, were used. Additionally, these constructs allowed easy reproduction of trials and served as an accurate representation of a monolayer. The fibronectin pattern generally inhibited translational

movement outside the circle; however, rearrangement of cells within the 100 µm circle resulted in measurable contractile forces.

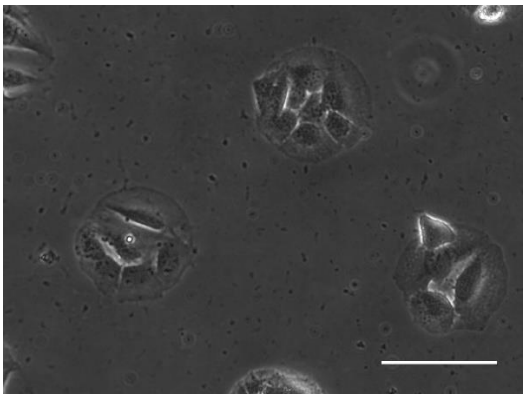

Figure 11. 100 µm HPMEC micro-patterns. Scale bar: 100 µm. Typically, each circle contained anywhere between two and six cells. Patterns with more than six were generally avoided as crowding eventually lead to cell death.

Figure 12 shows the average force generated by a negative control micro-pattern over a 90 min time period 24 hr after seeding. Overall, the average force remained consistent, with no statistically significant deviations. Six micro-patterns were randomly selected and imaged across two different gels. These two experiments provide a solid baseline for comparison to future HPMEC-A2058 studies.

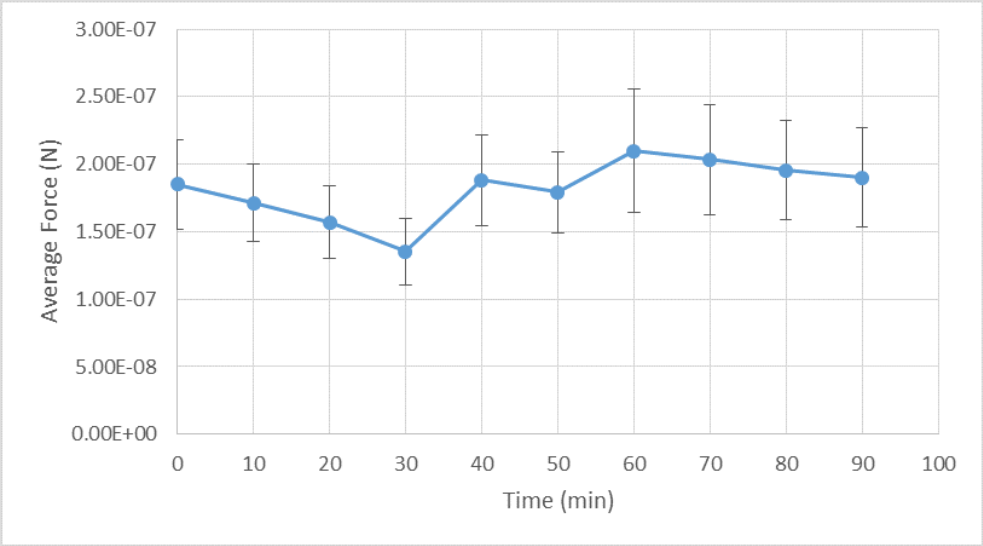

Figure 12. Averaged force (N) over time (min) for HPMEC micro-patterns 24 hr after seeding and untreated on 5 kPa PA gels (n=6). Forces were measured every 10 min with mean ± SEM reported. Generally, forces ranged between 0.15 µN and 0.2 µN across the 90 min time period. $p>0.05$ indicating no statistically significant differences between consecutive time points.

Performing these experiments with Virginia Aragon, HPMEC cells were incubated with metastatic A2058, with forces recorded at 0 min, 10 min, 45 min, and 90 min. Figure 13 shows representative bright field images from a time course experiment. As can be observed, extravasation did occur, with apparent gap formation at the 10 min mark. As time progressed, gaps grew larger with some cells even rounding and detaching from the substrate all together.

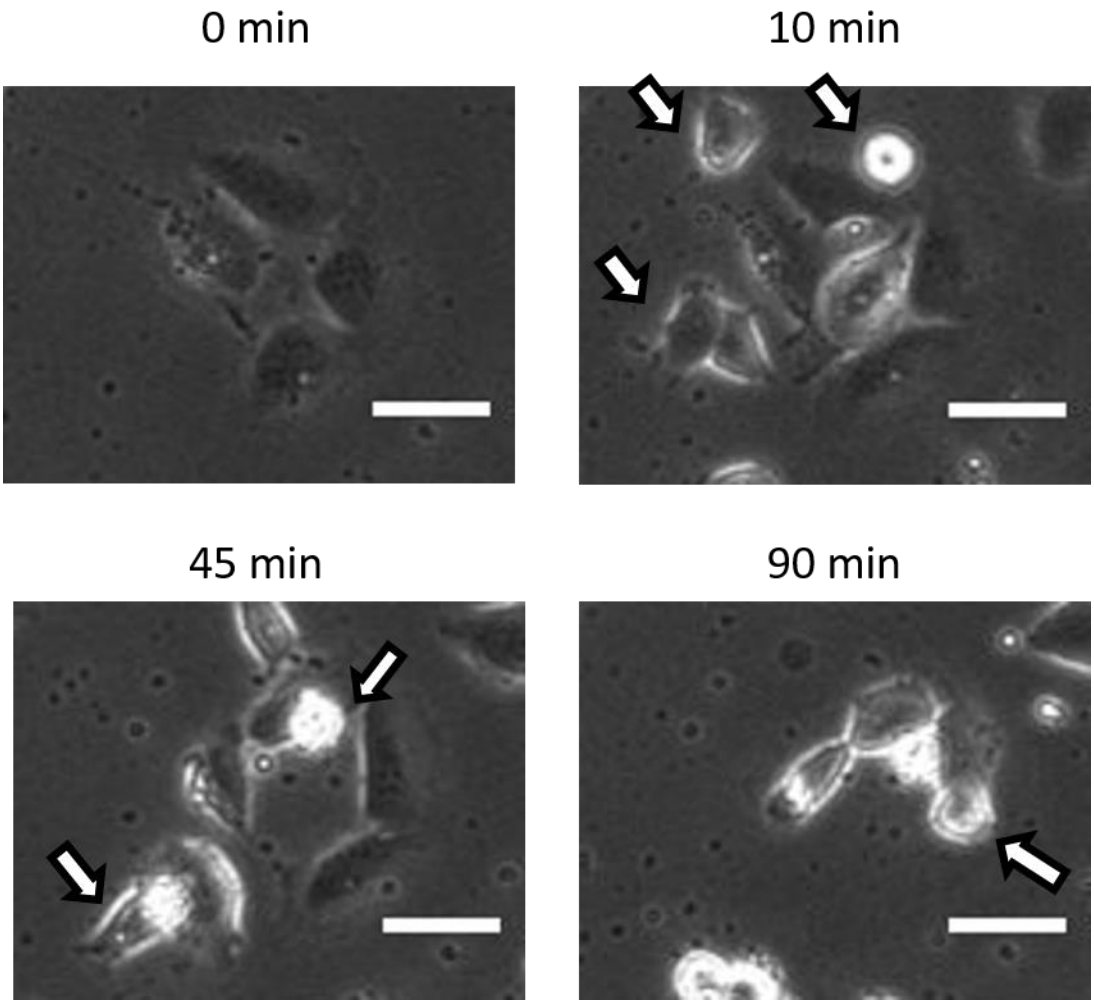

Figure 13. Representative bright field images of HPMEC-A2058 co-incubation traction force experiment. Endothelial cells were seeded into circular micro patterns and come into direct contact with A2058. Scale bar: 50 μm. A2058, denoted by the white arrows, induced gap formation in micro-patterns. With time, the gaps grew larger, supporting the time-dependent relationship between junction breakdown and exposure to melanoma seen in previous studies.[11]

The normalized forces measured by endothelial islands as a function of time during this co-culture are denoted in Figure 14. For each experiment, separate HPMEC-A2058 co-incubation gels, one for 10 min, one for 45 min, and one for 90 min, were used for comparison to a negative control gel (HPMEC alone). Contrary to what was expected, endothelial forces decreased in a time-dependent fashion as time progressed. Based on the previous control experiments, we determined that this change could be directly attributed to the contact between

A2058 and HPMEC cells. Overall, results from these traction force microscopy experiments suggested a time-dependent decrease in force transmission coinciding with an increase in gap formation. These results would also serve as a basis for future focal adhesion studies done in an effort to better study the mechanism by which melanoma cells caused this change and manipulated endothelial interactions with their substrate.

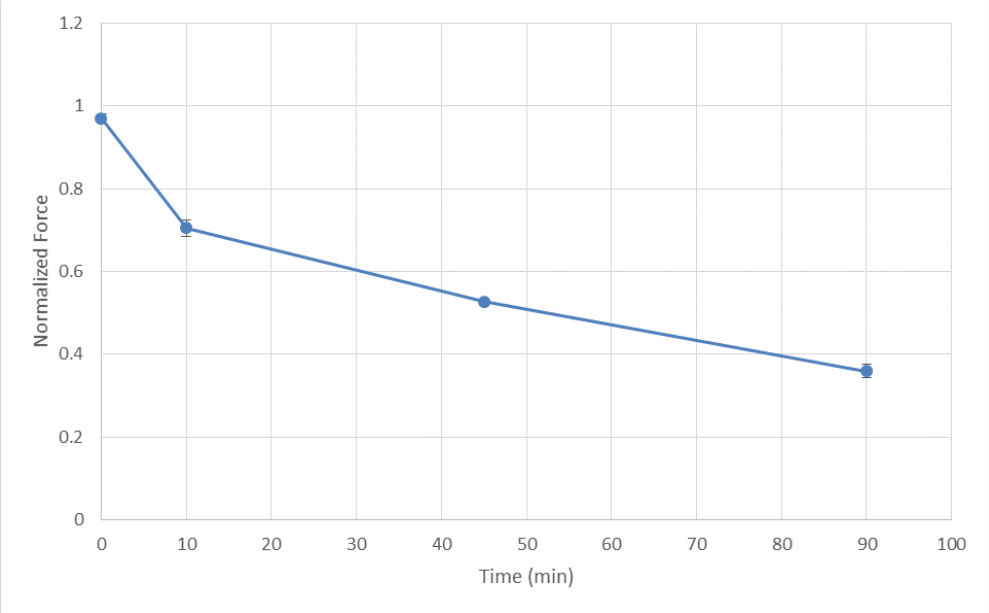

Figure 14. Normalized traction forces of HPMEC micro-patterns in direct contact with A2058 as a function of time. Each replicate constituted a negative control gel (0 min) and three co-incubation gels, one for 10 min, one for 45 min, and one for 90 min. Means ± SEM are reported (n= 20 micro-patterns). A clear reduction is shown with a large initial decrease recorded from the 0 min to 10 min mark.

3.2 Changes in Focal Adhesion Expression

Based on the previous TFM experiments, we looked to changes in FA expression as a possible explanation. As explained previously, adhesions serve as a bidirectional transductor, allowing the transmission of cytoskeletal forces to a substrate while receiving input from surroundings. To study this, micro-patterns of HPMEC cells in direct contact with A2058 were fluorescently stained for vinculin and F-actin. Figure 15 offers representative images of this experiment under three separate channels, GFP, TxRed, and DAPI, along with a merged picture. Focal adhesions, as seen in the "Vinculin" row of Figure 15, are observed as small, green fluorescent patches on the cell periphery. Actin filaments, as seen in the "Actin" row of Figure 15 are observed as long red fibers, with some seen to terminate at adhesion sites. FA complexes were not visible along endothelial cell-cell barriers. The negative control micro-patterns did not have any gaps between cells, forming a tight barrier. However, upon addition of melanoma, gaps started to form with micro-patterns breaking apart by the end of 90 min. One noteworthy aspect of these images is the presence of stress fibers near sites of melanoma attachment, especially noticeable at the 10 min mark in Figure 15. Concentrated actomyosin filaments are also visible at cellular protrusions, seen at the 90 min mark, indicative of attempted motility. A qualitative inspection showed a noticeable decrease in adhesion sites necessitating the need for quantitative analysis.

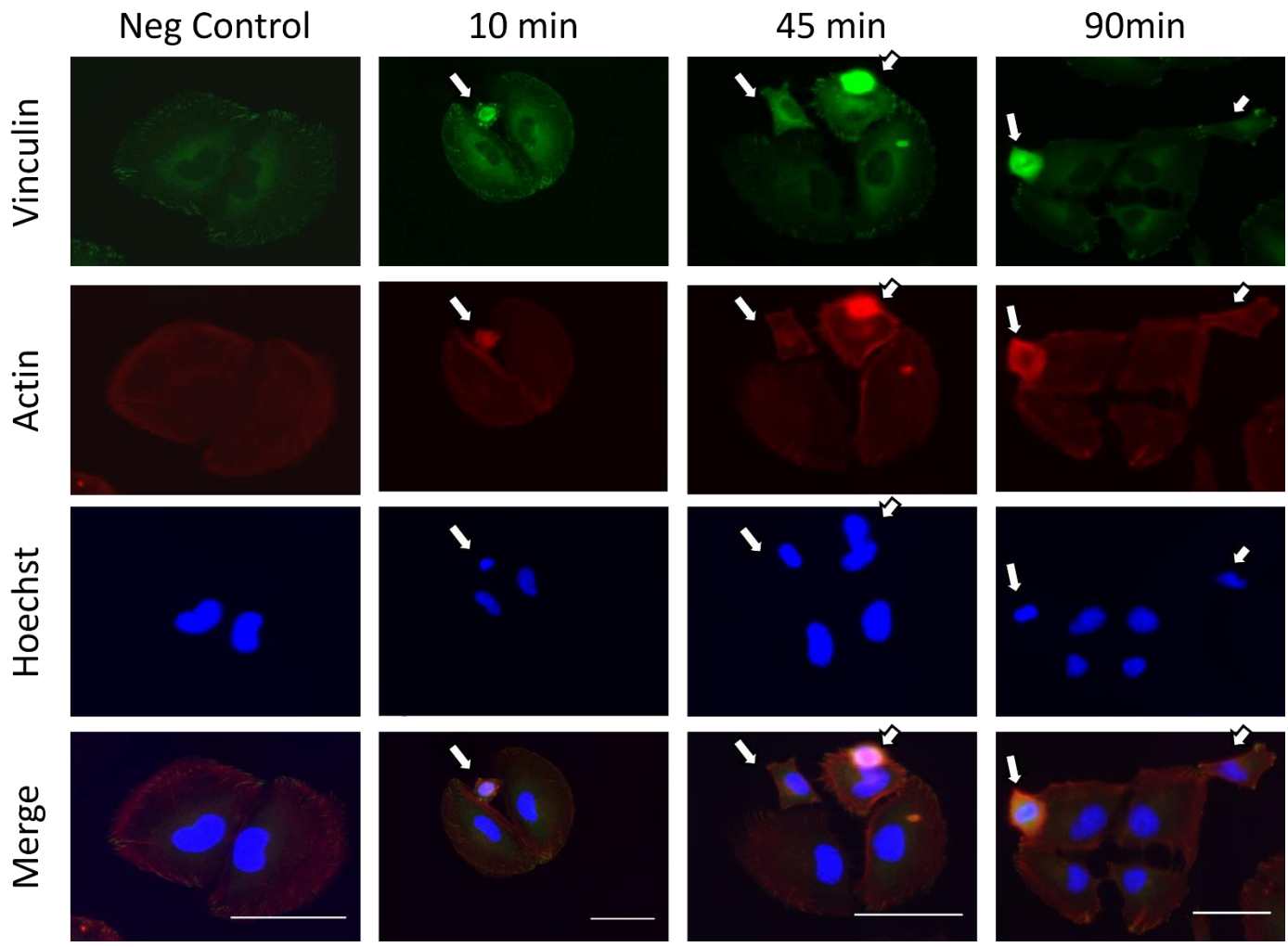

Figure 15. Metastatic melanoma incubated with micro-patterned HPMEC cells on a 5kPa PA gel for time points 10 min, 45 min, and 90 min. Cells were immunostained for vinculin (green) and F-actin (red). Scale bar: 50 µm. White arrows indicate metastatic A2058 cells.

Numerical analysis of the quantity and total area of adhesion sites was conducted with the FAAS. Through adjustment of the min/max and detection threshold, focal adhesions were delineated by yellow outlines, as seen in Figure 16. As observed during various trials, the frequent rounding of melanoma cells and their expression of focal adhesions within such a small area resulted in FA areas well above the maximum threshold, preventing erroneous inflation of results. This is also illustrated in Figure 16.

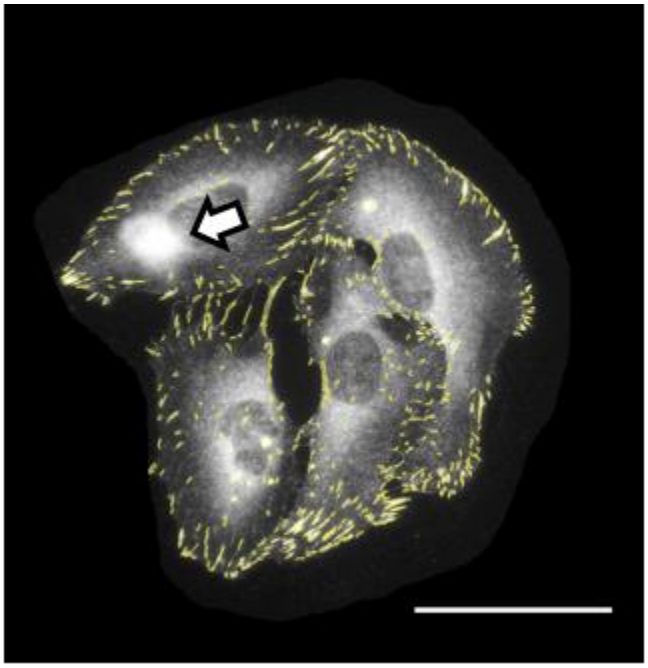

Figure 16. Representative, resultant picture of micro-pattern after analysis through FAAS. A boundary drawn beforehand in ImageJ allowed for the removal of background noise and FA identification outside of the target area. Scale bar: 50 μm. Metastatic A2058 cell, incubated for 45 min, is highlighted by the white arrow.

Figure 17 provides a quantitative description of focal adhesion disassembly over time. Each replicate constituted a negative control PA gel (0 min) and three co-incubation gels, one for 10 min, one for 45 min, and one for 90 min. The largest decrease, both in FA number and total FA area per cell, was observed between Time 0 (Negative Control) and 10 min, matching the trend observed in Figure 14 showing normalized traction forces. Statistical analysis in the form of an ANOVA and Tukey post hoc test showed a significant difference between the negative control and each time point (10 min, 45 min, and 90 min). While a significant difference existed between 10 min and 90 mins for focal adhesion number, this was not the case between 10 min and 45 min, and 45 min and 90 min. Interestingly, the downward trend between FA number and total FA area was very similar suggesting a close relationship between these two parameters. Overall, these results show a significant reduction in the number (Figure 17A) and total area of

focal adhesions (Figure 17B) per endothelial cell upon incubation with A2058. The gap percentage, as denoted in orange, was reproduced with permission from Virginia Aragon and the Dong lab. Gaps were measured by staining endothelial monolayers on glass slides for VE-Cadherin and dividing the area not covered by HPMEC cells by the total area of the image. These previously conducted experiments found a trend of increased gap formation as a function of time when metastatic A2058 comes into direct contact with an HPMEC monolayer. Based on the trend proposed by Figure 17, an increased presence of gaps in the endothelial layer coincides with decreased FA expression during co-incubation.

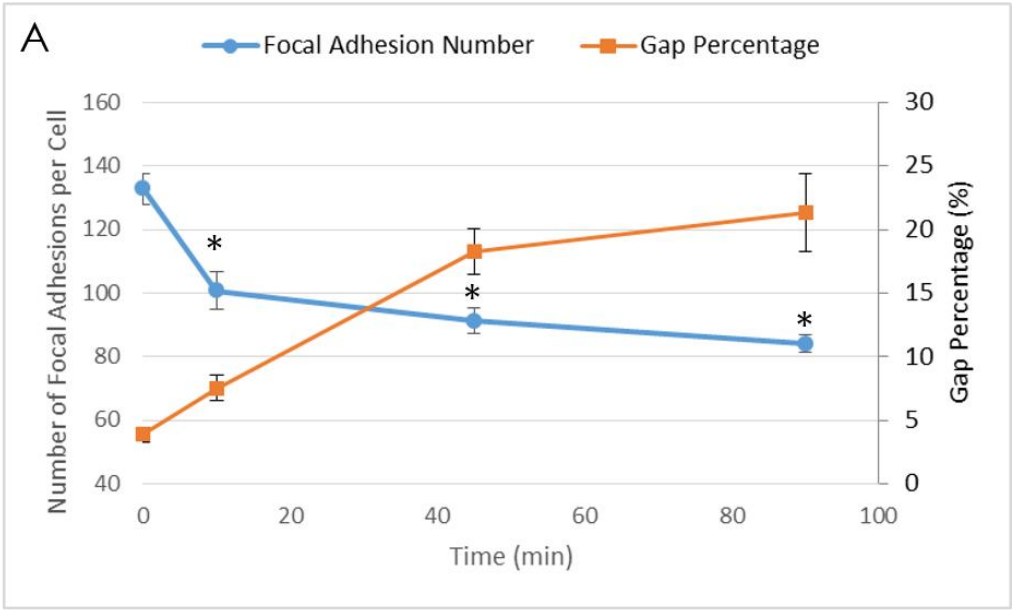

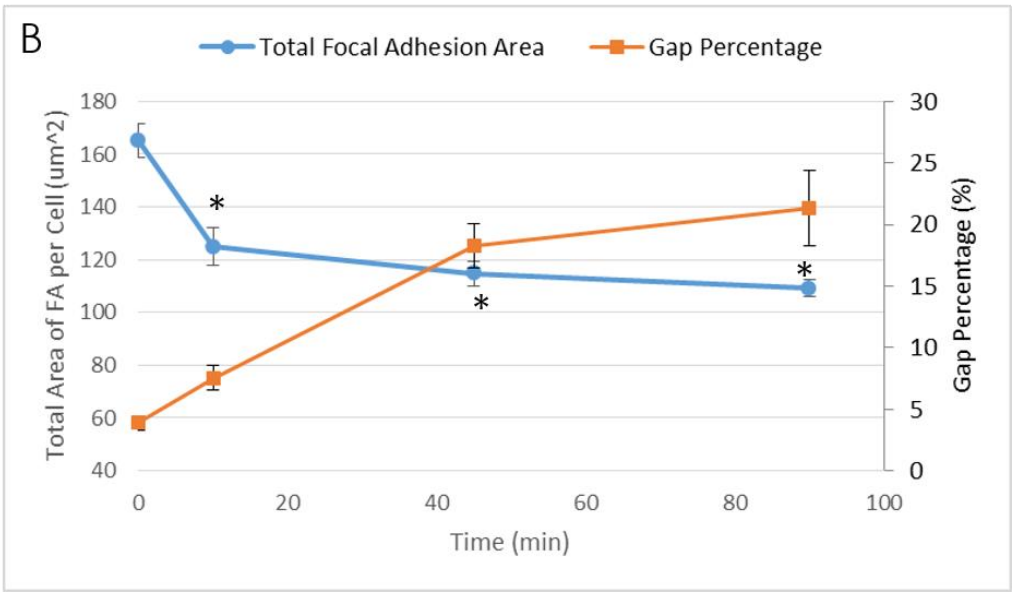

Figure 17. HPMEC gap percentage and FA expression after incubation with metastatic melanoma for 10 min, 45 min, and 90 min. (A) The total number of focal adhesions per cell calculated by summing the total number of FAs in one micro-pattern and dividing by the number of cells. (B) The total area of focal adhesions per cell calculated by summing the total area of individual adhesions and dividing by the number of cells. Plots represent the mean ± SEM. * indicates $p<0.05$ when compared to 0 min (negative control). No significance between 10 min and 45 min, and 45 min and 90 min for FA expression. (Adhesion Expression: Neg Control: n=32, 10 min: n=26, 45 min: n=30, 90 min: n=29 micro-patterns across four replicates; Gap Percentage: n=3 slides across three replicates)

In order to determine the role that Src played in the reduction of focal adhesion expression, an inhibitor, PP1 was added 2 hrs before experimentation. Figure 18 depicts representative images of a negative control pattern and a 90 min time point upon incubation with A2058. It is interesting to note that even after the 90 min mark, there was minimal gap formation and no noticeable changes in the organization of the actin cytoskeleton. As expected, there was a high concentration of adhesions along the outer periphery with little expression along endothelial cell-cell junctions.

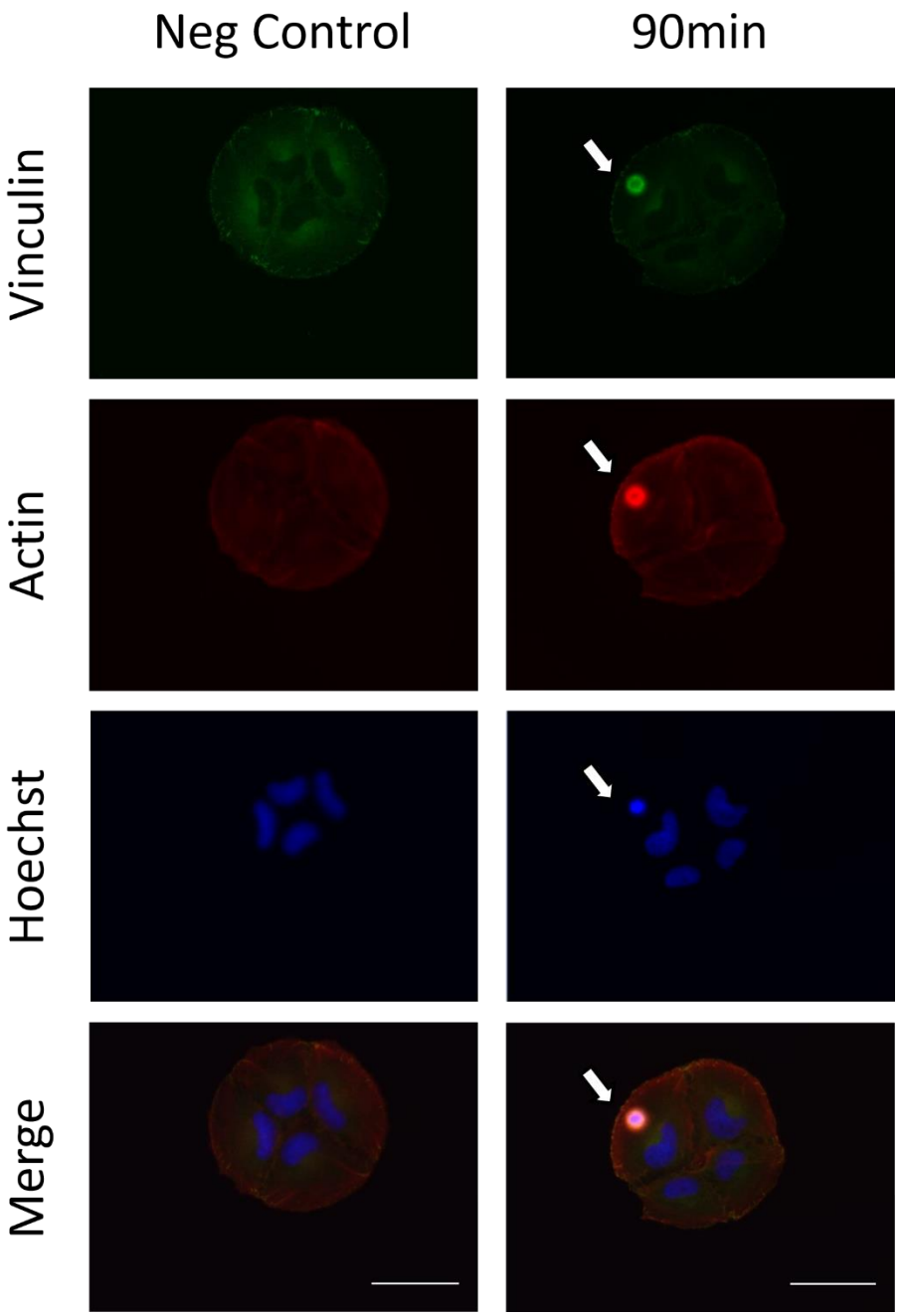

Figure 18. Immunostaining of HPMEC-A2058 co-incubation experiment with addition of 30 µM PP1 inhibitor. Scale bar: 50 µm. Cells were stained for vinculin (green) and actin (red). Two representative micro-patterns, one negative control and another after 90 min of direct contact with A2058 are shown. Melanoma cell denoted with white arrow.

Analysis of total FA number and FA area per cell, seen in Figure 19, showed no

significant reduction in expression between the negative control (Neg Control PP1+) and 90 min

time point (90 min PP1+). Comparing total FA numbers and areas of negative controls with and without PP1 (Neg Control PP1+ and Neg Control PP1-) using a Tukey post hoc test yielded no significant differences ($p>0.05$). However, a similar comparison after 90 min of incubation with A2058 did yield a statistical deviation ($p<0.05$) in both total FA number and FA area per cell. These results suggest that Src does in fact play an important role in adhesion disassembly and its inhibition can stymie this effect.

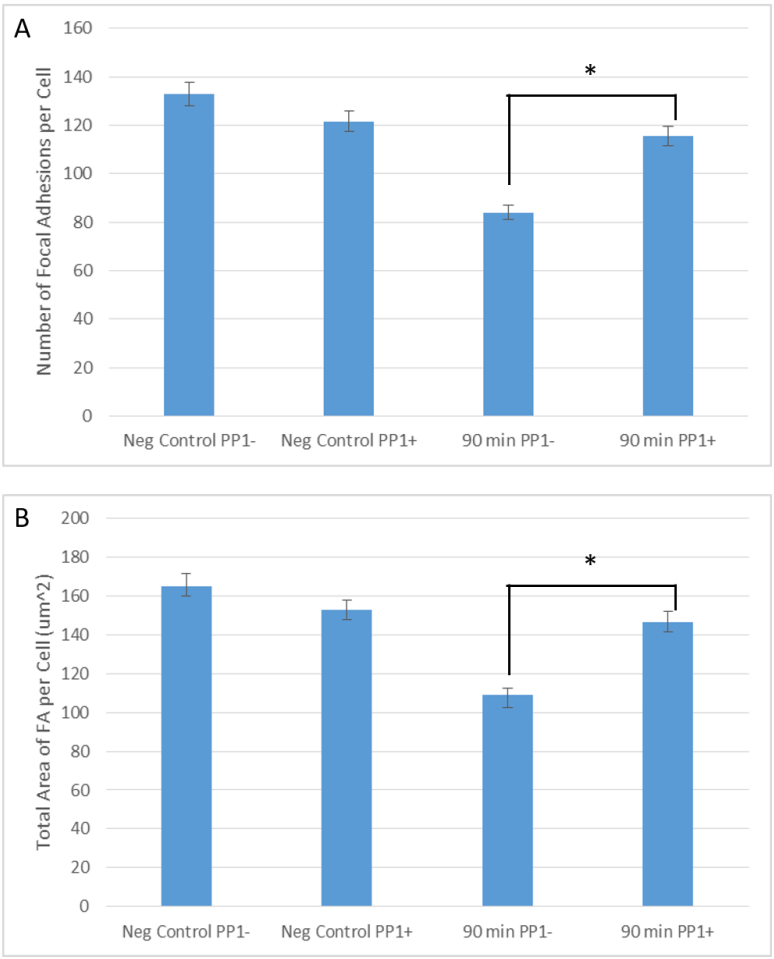

Figure 19. HPMEC micro-patterns with PP1 treatment (PP1+) and without (PP1-) prior to experimentation, either no treatment (Neg control) or 90 min incubation with A2058. (A) The total number of focal adhesions per cell and (B) the total area of focal adhesions per cell. Plots represent the mean ± SEM. For both plots, $p<0.05$ between the 90 min time point with and without PP1, indicating a statistically significant differences in means. (Neg Control PP1-:n=32, Neg Control PP1+: n=43, 90 min PP1-:n=29, 90 min PP1+:n=46 micro-patterns)

Chapter 4

Discussion

Melanoma extravasation has been shown to induce gap formation in the endothelial barrier.[37] The process is complex, involving ligand-receptor interactions and the secretion of soluble cytokines. Previous studies in our lab have found that the association of VLA-4 expressing cells with the VCAM-1 ligand on the endothelium promoted transmigration of melanoma.[15] This interaction led to VE-Cadherin phosphorylation, causing disassembly of adheren junctions, which are responsible for endothelial cell-cell attachment and barrier integrity.[11] These factors have also lead to apparent increased endothelial contractility via actin remodeling and the phosphorylation of myosin light chains, allowing for facile melanoma transmigration.[11]

This study expands on the described previous work by cultivating a better understanding of how this pathway manipulates endothelial cell interaction with its substrate. In terms of experimental design, single-cell experiments do not account for intercellular interaction present in a normal, healthy endothelium. Additionally, a monolayer is far too expansive, providing no frame of reference for bead displacement under a microscope making TFM difficult. These limitations necessitated cell seeding of an intermediate size in the form of micro-patterns, which yielded reproducible results while serving as an accurate representation of the endothelial barrier.

First, TFM experiments that measured normalized endothelial forces upon incubation with metastatic A2058 melanoma for 10 min, 45 min, and 90 min showed decreasing stresses with time, as seen in Figure 14. In order to ensure no confounding factors were responsible, control experiments conducted with just A2058 ensured these cells did not generate any contractile stress on their own. After, a baseline level of endothelial contractility was measured

over a 90 min period, as seen in Figure 12. As no significant perturbations during this time period were noted, the decrease in traction forces as a function of time could be directly attributed to the direct contact between melanoma cells and the endothelial layer. These results seemed counterintuitive at first to what was expected. For instance, a recent study measuring mechanical force during neutrophil transmigration found an increase over time, with maximal contractility roughly 1.5 min after cellular contact.[38] This discrepancy not only suggests an alternate mechanism for melanoma extravasation, but one that alters force transmission from cell to substrate.

As focal adhesions are an intermediary, conducting forces from the cellular cytoskeleton to integrins and the attached substrate, their expression in endothelial cells during the same 90 min time frame was studied. Vinculin has an essential role in adhesion assembly through its binding of talin and actin.[39] Additionally, it has been found that the tail domain of the protein is responsible for the functional link of focal adhesions to the cellular cytoskeleton.[39] For this reason, vinculin was chosen to be fluorescently tagged as a marker for focal adhesions. Measuring changes in vinculin's expression would therefore allow a direct comparison of actomyosin contractility and FA presence. Immunostaining of HPMEC micro-patterns in direct contact with A2058 found a reduction in both total FA number and total adhesion area per cell, as seen in Figures 17A and 17B. Interestingly, a larger decrease in measured traction force between the 0 min (negative control) and 10 min mark, Figure 12, was matched by a similar drop in both FA number and total adhesion area, Figure 17, relative to the trend seen from 10 min to 90 min. These results propose a close relationship between contractility and adhesion expression.

An upper and lower threshold of individual FA areas, at 20 and 400 pixels^2 respectively, was set to ensure a range wide enough to capture adhesions while disregarding large aberrations

and noise. These values corresponded to areas of 0.5 and 10.4 μm^2 respectively, keeping typical nascent FAs of 1-2 μm^2 and mature FAs of 6-8 μm^2 well within these bounds. As the quantity of adhesions is directly related to cell spreading, deviations in FA expression between cells are inevitable. The use of micro-patterns and selection of islands possessing between two and six cells were used in an attempt to control these differences; however, this methodology does represent a limitation of the study. Additionally, the use of fluorescent microscopy over confocal techniques resulted in noisy images, with atypical adhesion recordings along the periphery of the nucleus. This was partially mitigated through the use of a cytoskeletal stabilization buffer; however, analytic software still occasionally misreported FAs in certain micro-patterns.

To explain the mechanism of FA disassembly, it was hypothesized that over-activation of Src was directly responsible. The Src kinase has multiple roles in various cell signaling pathways, including adhesion, growth, survival, and differentiation. Studies have shown that integrin engagement can increase Src activity by dephosphorylating regulatory site pY527, leading to its migration to focal adhesions.[28] Src's SH2 and SH3 domains stabilize this localization, facilitating Src binding to FA proteins, including paxillin, FAK, and vinculin.[28] Src association with FAK leads to Src-mediated phosphorylation of tyrosine residues on FAK, increasing FAK activity.[28] Src-FAK complex activation includes promotion of Rac1, a GTPase implicated in the formation of cellular protrusions, and suppression of RhoA-GTP levels, relieving cytoskeletal tension during cell spreading.[24] Therefore, in addition to mediating FA turnover through local phosphorylation, Src-FAK complexes promote cell spreading through protrusion formation and inhibition of contractility.[24] Recent findings, in the form of an unpublished manuscript by the Dong lab, have also identified increased cellular Src activity as a

potential modulator for endothelial gap formation, activated by stimulation of the endothelial VCAM-1 protein and secretion of the cytokine IL-8 by cells with metastatic potential.

Addition of a Src inhibitor, PP1, and immunostaining of vinculin in endothelial micro-patterns resulted in no significant difference between FA number or total FA area between negative control (no treatment) and 90 min HPMEC-A20158 co-incubation trials. Interestingly, the decrease in FA number and total area observed at the 90 min time point was reversed with the addition of the inhibitor. These results suggest that suppression of Src prevented adhesion disassembly throughout extravasation. This is postulated to be a result of reduced Src-mediated phosphorylation of Tyrosine residues 100 and 150 on vinculin, which serves as a mechanism for the regulation of actin filament reassembly and motility and heightened Src-FAK activity.[29] Recent literature has suggested a similar trend in other cell lineages, as observed with the presence of an oncogenic, hyperactive v-Src in chicken embryo fibroblasts resulting in degradation of FAK and limited cell motility and spreading.[33] These results advance findings of Src's role as a regulator of endothelial adhesion expression and disassembly while supporting its critical role in melanoma metastasis.

Chapter 5

Conclusion and Future Work

Overall, this study serves to expand on our current understanding of the signaling cascade associated with melanoma metastasis. Through an interplay of transmembrane protein interactions and cytokine signaling, an endothelial cytoplasmic kinase, Src, is stimulated leading to disassembly of focal adhesions, and in turn, a reduction in force transmission from cell to substrate. This effect can be mitigated through Src kinase's inhibiton via PP1, highlighting its potential use as a therapy. The results shown offer additional insights into potential treatment options. Even beyond inhibition of the Src kinase, preventing the phosphorylation of adhesion proteins, such as vinculin or talin, could keep adhesions intact, mitigating gap formation and curbing metastasis.

Based on the results presented, there are many possible avenues for future study. One potential worthwhile cause may be through additional testing of these results with the use of micro-fabricated pillars. As a cell contracts, it causes the constructs to deform, allowing extrapolation of generated stress from displacement. These substrates have already been used in studies of epithelial migration and would allow for more refined visualizations of contractile stresses during migration.[40]

The next step would be to study the temporal relationship of these proteins on a more refined time scale. The FAAS server allows analysis of adhesion assembly and disassembly rates based on a stack of time course images of a single micro-pattern. Transfecting endothelial cells with fluorescently tagged FAK, which is directly responsible for FA construction, would allow quantification of these particular rates. Studying FAK concentrations could also lend better insight into its relationship with Src, specifically the Src-FAK complex, and provide a time-

dependent expression profile for comparison to experiments conducted here. The use of a fluorescence resonance energy transfer (FRET) sensor could also be a viable option, providing real time data on expression as a function of intensity during extravasation. A recent article published by Boudaoud et al. provides an ImageJ plugin "FibriTool" capable of quantifying fibrillary structures, specifically actin stress fibers, from vinculin and actin stained images.[41] The output generated, namely fiber orientation, anisotropy, and density, could be useful in studies of actin cytoskeleton reconstruction over time during extravasation.

Additionally, studying these variables under different environmental factors could provide a nuanced explanation of the metastatic pathway. For instance, the relationship between substrate stiffness and adhesion expression could not only better outline the mechanism for force transduction through FAs, but also serve to explain why some locations in the body may be more susceptible to extravasation. Performing similar experiments with different types of melanoma cells, such as WM35 a melanoma cell type with low incidences of induced endothelial gap formation, would also better characterize differences in adhesion expression as a function of metastatic potential.

Appendix A

Focal Adhesion Expression Data

Table 1. Focal adhesion expression of negative control HPMEC micro-patterns. Conversion of 0.1613 µm/pixel

# of Cells per MicroPattern	# of FA per Cell	Total FA Area per Cell (pixel^2)	Total FA Area per Cell (um^2)
2	100.00	7088.50	183.74
3	108.33	5040.67	130.66
4	127.50	5925.75	153.60
3	146.67	7296.00	189.12
4	121.25	4804.00	124.52
2	179.00	8672.50	224.80
3	133.67	5781.67	149.87
2	163.50	8484.00	219.91
2	165.50	7318.50	189.70
3	164.67	6806.00	176.42
4	127.50	5781.25	149.86
4	102.50	5233.75	135.66
4	124.50	4520.75	117.18
2	117.50	5509.50	142.81
5	81.60	3867.20	100.24
2	172.50	7965.50	206.47
2	127.00	7035.50	182.37
4	120.25	5471.00	141.81
4	142.00	7676.25	198.98
3	122.00	6402.67	165.96
2	139.50	5065.50	131.30
4	102.50	5233.75	135.66
3	122.00	6402.67	165.96
4	84.50	4520.75	117.18
3	163.67	5990.00	155.27
2	119.00	6224.50	161.35
3	140.33	7819.33	202.68
5	148.00	8307.80	215.35
4	198.50	9797.75	253.97
4	121.00	5559.75	144.11
4	132.25	7171.50	185.89
2	129.50	5065.50	131.30
Avg # of FA per Cell	132.76	Avg Total FA Area per Cell	165.12
Std Dev	26.84	Std Dev	36.58
Standard Error	4.75	Standard Error	6.47

Table 2. Focal adhesion expression of HPMEC micro-patterns incubated for 10 min with A2058. Conversion of 0.1613 µm/pixel

# of Cells per MicroPattern	# of FA per Cell	Total FA Area per Cell (pixel^2)	Total FA Area per Cell (um^2)
2	127.50	5735.00	148.66
2	150.00	4976.00	128.98
3	150.00	7980.00	206.85
2	105.00	4060.00	105.24
2	110.00	4718.00	122.30
3	77.33	3686.67	95.56
2	95.50	4519.50	117.15
4	96.75	4423.25	114.66
2	68.50	5276.50	136.77
4	153.00	7168.00	185.80
2	91.50	4339.00	112.47
4	89.25	5845.50	151.52
4	138.00	7042.25	182.54
3	112.33	5528.00	143.29
5	86.60	3445.80	89.32
4	106.50	4704.25	121.94
4	106.50	4932.50	127.86
3	24.33	1906.00	49.41
3	109.67	5558.67	144.09
3	89.00	4285.00	111.07
3	60.33	2731.33	70.80
3	108.33	6158.33	159.63
4	131.25	3854.25	99.91
3	107.67	5139.00	133.21
4	73.00	3950.00	102.39
4	74.00	3386.00	87.77
Avg # of FA per Cell	101.61	Avg Total FA Area per Cell	124.97
Std Dev	29.82	Std Dev	35.41
Standard Error	5.85	Standard Error	6.94

Table 3. Focal adhesion expression of HPMEC micro-patterns incubated for 45 min with A2058. Conversion of 0.1613 µm/pixel

# of Cells per MicroPattern	# of FA per Cell	Total FA Area per Cell (pixel^2)	Total FA Area per Cell (um^2)
4	76.00	3072.25	79.64
5	75.40	3367.80	87.30
2	98.00	4125.50	106.94
2	135.50	6043.00	156.64
6	134.33	6678.83	173.12
4	77.50	3354.25	86.95
2	62.50	3617.50	93.77
4	73.25	3993.00	103.50
4	89.75	4255.50	110.31
4	99.50	4874.75	126.36
4	95.50	4514.50	117.02
4	97.50	4616.00	119.65
4	73.75	3639.25	94.33
2	108.00	4785.50	124.04
3	104.33	4674.33	121.16
4	122.75	5611.25	145.45
5	81.20	4211.80	109.17
4	115.00	5837.75	151.32
5	71.80	3966.00	102.80
4	122.25	5476.25	141.95
3	48.00	2803.67	72.67
4	98.25	4417.25	114.50
4	91.00	5273.25	136.69
4	109.25	4932.25	127.85
3	75.33	4390.67	113.81
4	105.25	5308.00	137.59
4	67.50	3238.00	83.93
3	101.00	5030.67	130.40
4	85.50	4131.25	107.09
4	58.25	2594.50	67.25
Avg # of FA per Cell	91.27	Avg Total FA Area per Cell	114.77
Std Dev	21.82	Std Dev	25.55
Standard Error	3.98	Standard Error	4.66

Table 4. Focal adhesion expression of HPMEC micro-patterns incubated for 45 min with A2058. Conversion of 0.1613 µm/pixel

# of Cells per MicroPattern	# of FA per Cell	Total FA Area per Cell (pixel^2)	Total FA Area per Cell (um^2)
4	89.25	4677.50	121.25
6	86.17	4394.83	113.92
4	100.00	4732.25	122.66
2	72.50	4151.50	107.61
3	83.33	4506.33	116.81
6	68.50	3278.67	84.99
3	74.33	4403.67	114.15
3	112.00	5302.67	137.45
2	124.50	5886.00	152.57
3	72.00	3970.00	102.91
4	70.50	3476.25	90.11
4	101.00	4365.75	113.16
4	77.00	3965.00	102.78
5	63.20	3372.40	87.42
3	83.00	3924.00	101.71
2	89.00	4583.00	118.80
5	75.20	4443.60	115.18
5	79.80	3946.40	102.29
5	71.40	3728.60	96.65
6	99.50	5089.17	131.92
4	106.75	3910.25	101.36
4	86.50	4302.25	111.52
4	56.50	2627.00	68.09
4	99.75	5141.75	133.28
5	77.80	3777.40	97.91
4	85.25	4065.50	105.38
4	76.25	3389.50	87.86
2	69.50	4057.00	105.16
4	86.50	4699.50	121.82
Avg # of FA per Cell	84.08	Avg Total FA Area per Cell	109.20
Std Dev	15.13	Std Dev	17.27
Standard Error	2.81	Standard Error	3.21

Table 5. Focal adhesion expression of negative control HPMEC micro-patterns treated with PP1 for 2 hrs. Conversion of 0.1613 µm/pixel

#of Cells per MicroPattern	#of FA per Cell	Total FA Area per Cell (pixel^2)	Total FA Area per Cell (um^2)
2	123.00	5576.00	144.54
3	90.33	5159.33	133.74
3	110.33	5462.67	141.60
4	121.50	6202.75	160.78
3	121.33	5048.67	130.87
2	150.00	8295.50	215.03
4	72.50	3739.00	96.92
4	105.75	4962.25	128.63
2	113.00	4694.50	121.69
4	120.25	6595.50	170.96
4	108.50	5433.00	140.83
1	144.00	6886.00	178.49
2	125.00	6822.00	176.83
4	103.25	5040.25	130.65
3	107.33	5240.67	135.84
3	95.67	4851.67	125.76
2	118.00	5550.00	143.86
5	95.40	4719.20	122.33
3	105.33	5239.00	135.80
2	153.50	6811.50	176.56
2	182.00	9161.00	237.46
4	95.00	5082.25	131.74
4	99.50	5203.75	134.89
2	117.50	5752.00	149.10
4	116.75	5902.75	153.01
4	112.00	5179.50	134.26
2	105.00	6423.00	166.49
2	197.50	9078.00	235.31
2	202.50	8753.00	226.89
3	142.33	6657.67	172.57
2	147.00	6187.50	160.39
2	114.00	5253.50	136.18
3	154.00	7405.33	191.95
4	99.00	4222.25	109.44
3	84.33	4016.33	104.11
2	102.50	5775.50	149.71
3	116.00	5757.67	149.24
3	134.33	5680.67	147.25
3	155.33	7273.00	188.52
4	108.50	4746.00	123.02
4	102.25	5675.50	147.11
3	125.67	6283.67	162.88
3	125.33	6149.67	159.41
Avg #of FA per Cell	121.45	Avg Total FA Area per Cell	153.08
Std Dev	27.79	Std Dev	32.52
Standard Error	4.24	Standard Error	4.96

Table 6. Focal adhesion expression of HPMEC micro-patterns incubated with A2058 for 90 min after PP1 treatment for 2 hrs. Conversion of 0.1613 µm/pixel

# of Cells per MicroPattern	# of FA per Cell	Total FA Area per Cell (pixel^2)	Total FA Area per Cell (um^2)
2	183.50	9044.50	234.44
4	94.00	4817.00	124.86
4	81.25	3675.50	95.27
2	164.50	7074.00	183.37
3	104.67	5348.00	138.63
2	123.00	5781.50	149.86
2	134.00	6005.00	155.66
3	71.33	3417.33	88.58
4	86.50	4254.75	110.29
2	125.50	5647.50	146.39
4	82.50	4222.75	109.46
3	84.00	3783.00	98.06
3	102.33	5805.67	150.49
4	96.00	4770.50	123.66
4	56.50	3269.25	84.74
3	106.33	4716.33	122.25
2	190.00	9759.50	252.98
3	87.00	4869.33	126.22
2	128.00	6472.00	167.76
2	102.00	4371.50	113.31
2	94.00	5790.50	150.10
2	137.50	7354.50	190.64
2	125.00	5374.50	139.31
5	137.80	6794.40	176.12
3	123.00	5743.00	148.86
2	108.00	6183.50	160.28
3	110.67	5834.67	151.24
2	106.00	5616.00	145.57
3	115.00	5884.67	152.54
3	159.67	7205.00	186.76
2	178.00	9220.00	238.99
3	134.00	6317.67	163.76
4	92.50	3981.00	103.19
2	128.00	6826.00	176.94
4	107.25	5421.25	140.52
2	120.00	5287.50	137.06
2	125.50	5591.50	144.94
4	104.75	4464.00	115.71
2	95.50	4827.50	125.13
5	118.00	5639.40	146.18
2	144.50	7081.00	183.55
4	98.75	4870.00	126.24
3	108.33	5156.33	133.66
4	110.50	4565.75	118.35
4	102.50	6249.25	161.99
3	123.33	6046.00	156.72
Avg # of FA per Cell	115.46	Avg Total FA Area per Cell	146.75
Std Dev	27.88	Std Dev	36.12
Standard Error	4.11	Standard Error	5.33

BIBLIOGRAPHY

[1] Mendelsohn, John, et al. The Molecular Basis of Cancer. 4th ed. Philadelphia, PA: Saunders/Elsevier, 2014.

[2] Hanahan, Douglas, and Robert A Weinberg. “Hallmarks of Cancer: The next Generation.” *Cell* 144.5 (2011): 646–74.

[3] Jr, Gery P Guy et al. “Melanoma Treatment Costs.” *Amepre* 43.5 (2012): 537–545.

[4] Nordlund, J. J., and A. B. Lerner. “On the Causes of Melanomas.” *The American Journal of Pathology* 89.2 (1977): 443–448.

[5] Pound AW: Induced cell proliferation and the initiation of skin tumor formation in mice by ultraviolet light. J Pathol 2:269-275, 1970

[6] Poole, Catherine M., DuPont Guerry, and David Low. *Melanoma: Prevention, Detection, and Treatment*. Yale University Press, 2005.

[7] Hodi, F Stephen. “Well-Defined Melanoma Antigens as Progression Markers for Melanoma: Insights into Differential Expression and Host Response Based on Stage.” *American Association for Cancer Research* 12.3 (2006): 673–678.

[8] Liotta LA, Kohn E. Cancer Invasion and Metastases. *JAMA.* 1990;263(8):1123-1126.

[9] Vestweber, Dietmar, Andre Broermann, and Dörte Schulte. “Control of Endothelial Barrier Function by Regulating Vascular Endothelial-Cadherin.” *Current Opinion in Hematology* 17.3 (2010): 230–236.

[10] Mehta, Dolly, and Asrar B Malik. “Signaling Mechanisms Regulating Endothelial Permeability.” *Physiological Reviews* 86.1 (2005): 279–367.

[11] Weidert, Eric, et al. "Actinomyosin Contraction, Phosphorylation of VE-Cadherin, and Actin Remodeling Enable Melanoma-Induced Endothelial Cell-Cell Junction Disassembly." *PLoS One* 9.9 (2014): e108092. *ProQuest.*

[12] Mierke, Claudia Tanja. “Role of the Endothelium during Tumor Cell Metastasis: Is the Endothelium a Barrier or a Promoter for Cell Invasion and Metastasis?” *Journal of biophysics (Hindawi Publishing Corporation : Online)* 2008 (2008): 183516.

[13] Leckband, D.E., and J. de Rooij. “Cadherin Adhesion and Mechanotransduction.” *Annual Review of Cell and Developmental Biology* 30.1 (2014): 291–315.

[14] Garofalo, Angela et al. “Involvement of the Very Late Antigen 4 Integrin on Melanoma in Interleukin 1-Augmented Experimental Metastases.” *Cancer Res.* 55.2 (1995): 414–419.

[15] Liang, Shile, and Cheng Dong. “Integrin VLA-4 Enhances Sialyl-Lewisx/a-Negative Melanoma Adhesion to and Extravasation through the Endothelium under Low Flow Conditions.” *American Journal of Physiology. Cell Physiology* 295.3 (2008): C701–7.

[16] van Wetering, Sandra et al. “VCAM-1-Mediated Rac Signaling Controls Endothelial Cell-Cell Contacts and Leukocyte Transmigration.” *American journal of physiology. Cell physiology* 285.2 (2003): C343–52.

[17] Myers, C L et al. “Induction of ICAM-1 by TNF-Alpha, IL-1 Beta, and LPS in Human Endothelial Cells after Downregulation of PKC.” *American Journal of Physiology - Cell Physiology* 263.4 (1992): C767–C772.

[18] Murrell, Michael et al. “Forcing Cells into Shape: The Mechanics of Actomyosin Contractility.” *Nature reviews. Molecular cell biology* 16.8 (2015): 486–498.

[19] Maraldi, M., C. Valero, and K. Garikipati. “A Computational Study of Stress Fiber-Focal Adhesion Dynamics Governing Cell Contractility.” *Biophysical Journal* 106.9 (2014): 1890–1901. *PMC*.

[20] Style, Robert W et al. “Traction Force Microscopy in Physics and Biology.” *Soft matter* 10.23 (2014): 4047–55.

[21] Shen, Qiang et al. “Myosin Light Chain Kinase in Microvascular Endothelial Barrier Function.” *Cardiovascular Research* 87.2 (2010): 272–280.

[22] Burridge, K, and M Chrzanowska-Wodnicka. “Focal Adhesions, Contractility, and Signaling.” *Annual review of cell and developmental biology* 12 (1996): 463–518.

[23] Millard M, Odde S, Neamati N. Integrin Targeted Therapeutics. *Theranostics* 2011; 1:154-188. doi:10.7150/thno/v01p0154.

[24] Rottner, K, A Hall, and J V Small. “Interplay between Rac and Rho in the Control of Substrate Contact Dynamics.” *Current Biology* 9.12 (2016): S1–648.

[25] Laukaitis, Christina M et al. “Differential Dynamics of α5 Integrin, Paxillin, and α-Actinin during Formation and Disassembly of Adhesions in Migrating Cells.” *The Journal of Cell Biology* 153 .7 (2001): 1427–1440.

[26] Arnold, Kimberly M, Zoe M Goeckeler, and Robert B Wysolmerski. “Loss of Focal Adhesion Kinase Enhances Endothelial Barrier Function and Increases Focal Adhesions.” *Microcirculation* 20.7 (2013): 637–649.

[27] Goldmann, Wolfgang H. “Mechanotransduction and Focal Adhesions.” *Cell Biology International* 36.7 (2012): 649–652.

[28] Thomas, S, and J Brugge. “Cellular Functions Regulated by Src Family Kinases.” *Annu Rev Cell Dev Biol* 13 (1997): 513–609.

[29] Westhoff, M A et al. “Src-Mediated Phosphorylation of Focal Adhesion Kinase Couples Actin and Adhesion Dynamics to Survival Signaling.” *Mol Cell Biol* 24.18 (2004): 8113–8133.

[30] Hanks, Steven K et al. “Focal Adhesion Kinase Signaling Activities and Their Implications in the Control of Cell Survival and Motility.” *Frontiers in bioscience : a journal and virtual library* 8 (2003): d982–96.

[31] Mitra, Satyajit K., Daniel A. Hanson, and David D. Schlaepher. “Focal Adhesion Kinase: In Command and Control of Cell Motility.” *Mol Cell Bio* 6.January (2005): 56–68.

[33] Fincham, V. J., and M. C. Frame. “The Catalytic Activity of Src Is Dispensable for Translocation to Focal Adhesions but Controls the Turnover of These Structures during Cell Motility.” *EMBO Journal* 17.1 (1998): 81–92.

[34] Style, Robert W et al. “Traction Force Microscopy in Physics and Biology.” *Soft matter* 10.23 (2014): 4047–55.

[35] Hersen, Pascal, and Benoit Ladoux. “Biophysics: Push It, Pull It.” *Nature* 470.7334 (2011): 340–341.

[36] Stroka, Kimberly M, and Helim Aranda-Espinoza. “Endothelial Cell Substrate Stiffness Influences Neutrophil Transmigration via Myosin Light Chain Kinase-Dependent Cell Contraction.” *Blood* 118.6 (2011): 1632–40.

[37] Dong C, Slattery MJ, Liang S, Peng H-H. Melanoma Cell Extravasation under Flow Conditions Is Modulated by Leukocytes and Endogenously Produced Interleukin 8. *Molecular & cellular biomechanics : MCB*. 2005;2(3):145-159.

[38] Rabodzey A, Alcaide P, Luscinskas FW, Ladoux B. Mechanical Forces Induced by the Transendothelial Migration of Human Neutrophils. *Biophysical Journal*. 2008;95(3):1428-1438.

[39] Humphries, Jonathan D et al. “Vinculin Controls Focal Adhesion Formation by Direct Interactions with Talin and Actin.” *The Journal of Cell Biology* 179 .5 (2007): 1043–1057.

[40] du Roure, Olivia et al. “Force Mapping in Epithelial Cell Migration.” *Proceedings of the National Academy of Sciences of the United States of America* 102 .7 (2005): 2390–2395.

[41] Boudaoud, Arezki et al. “FibrilTool, an ImageJ Plug-in to Quantify Fibrillar Structures in Raw Microscopy Images.” *Nat. Protocols* 9.2 (2014): 457–463.

ACADEMIC VITA

Vikram Eswar

vxe5008@psu.edu

EDUCATION **Bachelor of Science in Biomedical Engineering**
The Pennsylvania State University, State College, PA *Dean's List (2012-Present)*
Schreyer Honors Scholar

RESEARCH **Cellular Biomechanics Laboratory** **2014-Present**
Research Assistant

- Helped elucidate role of endothelial membrane protein VE-Cadherin in melanoma extravasation as part of a paper to be submitted for publication
  - Carried out immunofluorescence staining of human pulmonary endothelial cells to detect Src and VE-Cadherin
- Performed traction force microscopy experiments to explore cellular contractility upon stimulus from cytokine IL-8 and A2058 melanoma cells as part of thesis research
  - Constructed polyacrylamide gels of physiological stiffnesses which were used for micropatterning

WORK EXPERIENCE **Anesthesia Services, P.A.** **May-August 2014**
Strategic Initiatives Intern

- Collected and recorded over 3,000 PONV study forms as part of a study to determine PACU efficiency
- Mapped practitioner, administrative, and nursing workflows to find redundancies in daily operating procedures and streamline schedules
- Assisted in development of online perioperative surgical assistance system that consolidated medical history forms, consultations, and post-operational follow-ups

Penn State Biology Department **2013-Present**
Lead Teaching Assistant

- Taught 16 students a wide range of biological concepts, from basic neural conduction to exercise physiology, as part of a 1 credit introductory biology lab
  - Graded lab reports and weekly quizzes
  - Led experiments involving EEG, EMG, frog dissections, pulmonary physiology, the senses, renal systems, and homeostatic mechanisms

SOFTWARE Solidworks, Mimics, MATLAB, COMSOL, Microsoft Office Suite, athenahealth

ACTIVITIES

- Patient floors volunteer at Mount Nittany Medical Center | Summer 2015
- Member of Rules and Regulation committee for Penn State IFC/Pan-Hellenic Dance Marathon | Fall 2012-Spring 2015
- Member of Tau Beta Pi (National Engineering Honors Society)
- Member of National Society of Leadership and Success